CLM-R248

CLM-R248

UKAEA

Report

ADVANTAGES AND DISADVANTAGES OF HIGH-POWER-DENSITY FUSION REACTORS

FIRST WALL THERMAL-MECHANICAL LIMITS

P. I. H. COOKE
R. A. KRAKOWSKI

CULHAM LABORATORY
Abingdon Oxfordshire
1984

C/18

Available from H. M. Stationery Office

£5.00

ADVANTAGES AND DISADVANTAGES OF HIGH-POWER-DENSITY FUSION REACTORS

FIRST WALL THERMAL-MECHANICAL LIMITS

P.I.H. Cooke and R.A. Krakowski*
Culham Laboratory, Abingdon, Oxon OX14 3DB, UK.
(Euratom/UKAEA Fusion Association)

ABSTRACT

The advantages and disadvantages of compact, high power density fusion reactors are examined by coupling a thermal-mechanical first wall model to a simple economics model based on costings contained in recent comprehensive fusion reactor studies. The benefits of compact devices result from the reduced size, and hence cost, of the first wall, blanket, shield and coils. The disadvantages include the more frequent replacement of the first wall and blanket, leading to a reduced availability and increased operating costs, and a lower coolant temperature and higher pumping power, resulting in a reduced overall thermal efficiency.

The analysis leads to a general relationship between the first wall loading and relative generating costs. Access to different ranges of wall loading is dependent on the thermal-mechanical performance as the first wall operating conditions (material, temperature, etc.) govern the maximum heat loading allowed. Two materials are considered for the first wall, a copper alloy and stainless steel. The thermal-mechanical results show that the copper alloy allows higher surface heat fluxes than stainless steel, typically 3 - 5 MW/m^2 compared with 0.3 - 0.5 MW/m^2. When related to the economic results these higher fluxes imply a potential for higher wall loadings and lower overall costs for reactors employing a copper alloy first wall. However, the materials database for copper alloys requires considerable expansion before this promise can be realised.

* Los Alamos Scientific Laboratory, PO Box 1663, Los Alamos, New Mexico 87545, USA.

July 1984

ISBN 085311 131 6

CONTENTS

1. INTRODUCTION

Most conceptual designs of fusion reactors have suggested that such devices will be large, with power densities considerably lower than for fission reactors. Capital cost estimates for these conventional fusion reactors have been correspondingly high. There has thus been interest in the so-called "compact" fusion reactors which would operate at power densities comparable with those of fission reactors with the accompanying economic advantages.

Attainment of the operational and economic benefits claimed[1,2] for compact, high power density fusion systems of acceptably small total power output will largely be determined by the performance of the first wall, where this term includes limiter, divertor, and other vacuum and plasma boundary surfaces subjected to high energy fluxes. Although some studies have addressed the performance of specific high heat-flux first wall designs[3,4], the majority of studies[5-10] give generic treatments of the problem. Generally, simplified models describing the thermal-mechanical response of an idealised first wall configuration are used to establish lifetime limits for a range of heat fluxes, coolants and material choices. The present study is also based on simplified models, but costing and reactor operational models are developed and applied to examine specific costs and benefits associated with high heat-flux systems.

The major questions which should be considered in any generic study include:

- Limitations imposed by the material strength under primary (coolant pressure) loads (yield, ultimate, and creep-rupture strengths)

- Limitations imposed by the material strength under cyclic loads (fatigue damage resistance, flaw and crack growth, related primarily to thermal cycles)

- Limitations due to thermophysical properties (heat transport and strength properties)

- Peak operating temperature (high-temperature strength, corrosion limits, tritium compatibility)

- Radiation resistance (He and H production, void and helium swelling, radiation-induced or enhanced creep, embrittlement), alloy alteration and physical property changes induced by transmutations

- Response to electromagnetic pulses and forces

- Physical and chemical sputtering, hydrogen isotope solubility, hydrogen recycle, other plasma-wall interactions

- Short-term (afterheat and maintenance considerations) and long-term (radwaste) radioactivity

- Commercial experience, fabrication, abundance and resource, cost.

Because of the complexity of the problem, the number of variables involved, and the general deficiency of experimental data, quantitative analysis of the first wall tends to focus on the first four issues[5-10]. Evaluations of the first wall performance are then made on the basis of idealised models and for a range of alloy and coolant combinations. The more difficult, but relevant, task of directly assessing the overall cost-benefit of high heat-flux operation of a given first wall configuration has largely been ignored.

The advantages of high power density reactor designs are related to the reduced size of the "fusion power core" (FPC), which includes the first wall, blanket, shield and coils. These benefits are the increased system power density, reduced mass and cost, and a reduced role played by the fusion power core in the total cost of a fusion reactor.

The problems associated with such designs have to be set against these merits. The disadvantages of high heat-flux first walls include:

- Derated coolant temperature leading to a reduction in overall plant efficiency

- Increased coolant pumping power, also contributing to the reduction in overall plant efficiency

- More complex designs with higher unit costs

- Reduced useful life, more frequent first wall replacement, reduced availability, and increased operating cost

These factors adversely affect the unit direct cost (UDC, total direct capital cost per unit electrical power output) and the cost of electricity (COE, generating cost per unit of electrical energy produced). At some point these increased costs will overwhelm the cost reduction related to a more efficient, cost-effective fusion power core, and a net increase in capital or generating cost will occur.

In order to assess this cost trade off, simplified models of the first wall thermal-mechanical response are used. These models differ little from those commonly used(3-10) to forecast generic material/coolant/lifetime trade offs. No attempt is made to match the level of detail included in some recently published first wall lifetime codes(11,12), which generally require more detailed design input and are restricted in the breadth allowed by any parametric survey. The mechanical constraints imposed in the analysis are similar to those used in the earlier studies, and are not as profound as would be allowed by the extensive stainless steel data base(13). The range of materials and coolants considered, however, is restricted in order to include in the analysis the cost-benefit trade off examined in terms of capital or generating cost. Specifically, only stainless steel and high-strength copper alloys are considered, both being cooled by pressurised water because of the emphasis placed on high-heat-flux operation. Of necessity, the costing models are highly condensed, although these simplified models are calibrated and tested against a number of recent comprehensive reactor studies.

The models used in this study are described in section 2 and

include the first wall and fusion power core energy-balance, the thermal-mechanical model and the global economics and costing models. The results are given in section 3 but do not include constraints anticipated for sputter erosion, bulk radiation damage, or specific creep/fatigue/fracture mechanical models, the inclusion of these effects remains as an area of future work. Results from a separate but similar study[14] which does enforce explicitly a fatigue and sputtering constraint are included, however. The economic results are presented as curves of generating cost (COE) as a function of wall loading. The form of these curves is insensitive to variations in the major parameters until a constraint (e.g., stress limit) is encountered, when either the cost increases rapidly or a given set of design parameters cannot be achieved for the constraints imposed. The effect is to present a nominally "universal" cost curve with the imposition of major constraints and fixed system variables (i.e. first wall material, coolant pressure, coolant-tube diameter, peak material temperatures and stresses, etc) limiting access to regions of the cost curve rather than defining new ones. With these universal cost curves defined, the analysis reported in this paper focuses onto the definition of specific operating regimes as defined by first wall heat flux, geometry, operating conditions, and materials, as dictated by thermal-mechanical and pumping power constraints.

2. MODELS

2.1 Thermal Model

The first wall is represented by a simple tube array, behind which is a blanket, shield and coils, as illustrated in fig.1. The coolant tube has an inner diameter d and the wall thickness is δ. The blanket and shield total thickness is Δb and the coil structure has a thickness Δc. The first wall minor radius is r_w, and the system radius is $r_s = r_w + \Delta b + \Delta c$, which, along with the major radius, R_T, defines the fusion power core volume, VFPC $= 2\pi^2 r_s^2 R_T$ (for a torus of circular cross-section). In calculating the average heat flux incident onto a first wall coolant tube the heat, particle and neutron flux is assumed to be

spread uniformly over the half-circumference and is thereby reduced by the form factor $\sim \pi/2(1 + 2\,\delta/d) \simeq \pi/2$. Neither stress enhancement nor residual thermal stresses related to the non-uniform irradiation of this tube bank(15-17) is taken into account. When computing critical heat fluxes [18], however, the average heat flux without reduction by this form factor is used, along with the heat flux "compression" caused by: (a) the decrease in tube outer radius $d/2 + \delta$ to inner radius $d/2$ and (b) the transport of nuclear volumetric heating across the inner radius to the coolant.

Throughout this study an ignited D-T plasma is assumed from which the total power density incident onto the scrape-off or plasma-edge region is equal to the alpha-particle power, $I_\alpha \simeq I_w/4$, where $I_w(MW/m^2)$ is the fusion neutron first wall loading. The fraction f_{RAD} of the alpha particle power is assumed to be radiated uniformly over the first wall tube bank, and of the remaining $(1-f_{RAD})$ particle energy flux the fraction f_L is assumed to be removed to a divertor duct or a limiter slot or surface. This energy split between first wall, blanket and limiter or divertor is also depicted on fig.1. Hence, the heat flux onto the first wall is given by

$$I_{Qw} = \frac{1}{4}\, I_w \,[1 - f_L(1 - f_{RAD})] \,. \qquad (1)$$

In addition, a uniform volumetric power density, $q(MW/m^3)$ is assumed to be deposited by neutron and gamma-ray heating in the coolant tube wall. Typically q/Iw lies in the range 8 to 12 m^{-1} for a wide range of first wall and blanket materials and configurations. The fraction of the total fusion energy deposited into the first wall tube array, therefore, is given by

$$f_{FW} = \frac{1 - f_L(1 - f_{RAD}) + 4\pi\delta\, \frac{d + \delta}{d + 2\delta}\, (q/I_w)}{4M_N + 1} \,, \qquad (2)$$

where M_N is the blanket energy multiplication for the fusion neutron. For the evaluation of critical heat flux limits, however, I_{Qw} is assumed to be geometrically enhanced at the coolant tube inner bore by the following factor

$$f_{CHF} = 1 + 2\delta/d + 4(q/I_w)\delta \frac{(1 + \delta/d)}{1 - f_L (1 - f_{RAD})}. \qquad (3)$$

The peak tube and average coolant temperatures are taken as T(O) and T_c, respectively, evaluated at the point where the coolant stream exits the first wall region. As seen from fig.1, the coolant at temperature $T_c < T_{BLK}$ is assumed to be used for feedwater heating under the assumption that the first wall conditions will limit the quality of thermal energy that can be delivered to the thermal cycle. Under these conditions the overall thermal conversion efficiency, η_{TH} , will depend on the temperature of the intermediate heat exchanger fluid $T_{IHX} = T_{BLK} + \Delta T_{IHX}$, T_c, and f_{FW} [equation (2)]. Since the dependence $\eta_{TH}(T_{IHX}, T_c, f_{FW})$ generally can be evaluated only once all state variables are specified for a particular thermal conversion cycle, this dependence cannot be parameterised conveniently. A particular example based on the general system depicted in fig.1 has been examined parametrically[19] and is used here to couple first wall performance and the overall plant thermal efficiency, η_{TH}, and hence generating cost. In this case the first wall pressurised-water coolant is used for feedwater heating, the IHX enthalpy drives a three-stage turbine (three stages of re-heat) with turbine, pump, and generator efficiencies of 88%, 75% and 95%, respectively, and $\Delta T_{IHX} = 30$ K. Under these conditions, the dependence of overall plant thermal efficiency $\eta_{TH}\ (T_{IHX}, T_C, f_{FW})$, is given by

$$\eta_{TH} = \eta^{o}_{TH} - \eta'_{TH}\, f_{FW} \qquad (4a)$$

where $$\eta^{o}_{TH} = 0.09 + 4.12(10)^{-4}\, T_{IHX} \qquad (4b)$$

and $$\eta'_{TH} = 0.74 - 1.17(10)^{-3}\, T_c\ , \qquad (4c)$$

where absolute temperatures (K) are used and the ranges of validity for T_c, T_{IHX}, and f_{FW} are, respectively, 425 → 625 K, 675 → 775 K, and 0 → 0.4.

Lastly, the overall temperature change in the coolant after passing through a tube of heated length L is given by

$$\frac{\Delta T}{L} = \frac{\left[1 + \frac{2\delta}{d}\right] I_w \left[I_{Qw}/I_w + \pi\delta \frac{1 + \delta/d}{1 + 2\delta/d} (q/I_w)\right]}{(\pi/4)\, c_p \mu_c Re}, \qquad (5)$$

where μ_c is the coolant viscosity, c_p is the coolant specific heat capacity, the Reynolds number is $Re = ud\rho_c/\mu_c$, and I_{Qw}/I_w is given by equation (1). These properties are summarised in Table I for the pressurised-water coolant considered. If P_{TH}(MWt) is the total thermal power, then the number, N, of first wall coolant tubes of length L is given by

$$P_{TH} = I_w(M_N + \tfrac{1}{4})L(d + 2\delta)N, \qquad (6)$$

which can be used along with equation (5) to estimate L and N as measures of system complexity and reliability.

2.2 Thermal-Mechanical Model

The analyses reported in References 4-13, generally identify a design window based on the relationship between an allowable heat flux, I_{Qw}, and a creep or fatigue stress limit for a given coolant tube geometry. For instance[9], either a simplified application of the ASME code criteria[20] is used, or the allowable stress is equated to a function of the yield stress, σ_Y, or the ultimate tensile stress, σ_U. Generally, the ASME code case given in Reference 20 operates on the basis of the following seven failure modes

- ductile rupture under short-term loads
- creep rupture under long-term loads
- creep-fatigue failure
- gross distortion from incremental collapse (ratchetting)
- loss of function because of excessive deformation
- buckling under short-term loads
- creep buckling under long-term loads

The second, third and fourth failure modes are most applicable to

the present problem. Failures resulting from sputter erosion, chemical corrosion, stress corrosion cracking, fatigue crack growth, radiation creep, or radiation swelling are not included. Because of the broad scope of the economically based parametric analysis and the considerably reduced data base for copper alloy when compared with stainless steel, the level of detail suggested by the Reference 13 analysis is not possible. Instead, the present model either parametrically specifies the ratio $\sigma/\sigma_Y = (\sigma_{TH} + \sigma_p)/\sigma_Y$, where σ_{TH} is the thermal (secondary) thermal stress and σ_p is the pressure (primary) stress, or limits the cyclic secondary strain, ε_{TH}. The effects of fatigue and creep on first wall life, or the method by which the coolant tube is pinned or otherwise constrained, therefore, can be lumped into the specification of σ/σ_Y or ε_{TH}.

The analysis of elastic-plastic behaviour of internally-pressurised thin-walled tubes suggested by Bree[21] for fission reactor fuel elements is applicable to the fusion reactor first-wall problem. Regions of elastic response, plastic cycling, thermal ratchetting, and the shakedown region between elastic and plastic or ratchetting behaviour can be identified on a plot of primary (pressure) stress versus secondary (thermal) stress; when these stresses are normalised to the yield stress, and the above regions are delineated, the so-called "Bree diagram" results[20,21]. The boundaries between the elastic (E), shakedown (S1,S2), plastic (P), and ratchetting (R1,R2) regions are given by the following expressions, where $X = \sigma_p/\sigma_Y$ and $Y = \sigma_{TH}/\sigma_Y$.

E/S1 boundary	$X + Y = 1$	(7a)
S1/R1 boundary	$X + Y/4 = 1$	(7b)
R1/R2 and S1/S2 boundaries	$Y(1 - X) = 1$	(7c)
S2/P boundary	$Y = 2$	(7d)
P/R2 boundary	$XY = 1$	(7e)

Hence, the specification of the stress ratio $\sigma/\sigma_y = X + Y \leqslant 1$ simply gives surfaces on the Bree diagram that are deeper into the elastic region. The various regions defined by equations (7) can also be translated onto a plot of I_{Qw} versus δ, this so-

called modified-Bree diagram[13] being adopted for this study. In the (S1,S2) and P regions of the Bree diagram, an effective creep stress, $\sigma_c \leq \sigma_y$ can be defined[13,22] to delimit the region of creep ratchetting using elastic analysis. The following additional surfaces on the Bree diagram result, where generally σ_c/σ_y is specified.

$$\sigma_c/\sigma_y = Y + 1 - 2\,[(1 - X)Y] \qquad S1 \qquad (7f)$$

$$\sigma_c/\sigma_y = XY \qquad S2 \qquad (7g)$$

Generally, the condition $\sigma/\sigma_Y = X + Y < 1$ is conservative in that operation is thereby restricted to the elastic regime, whereas the ASME code criterion allows some plastic deformation and work hardening[9]. Ultimately, the adaption of the damage function[23], the relationship with creep and fatigue life, the interactions between fatigue and creep, and most importantly, the effect of radiation damage and sputter erosion must be taken into account.

Before the primary and secondary stresses can be determined, the coolant pressure and the steady-state temperature distribution through the tube wall must be specified. Under the assumption of constant properties, steady state, and uniform heat flux, the following expression gives the first wall temperature gradient

$$\Delta T_w = T(0) - T(\delta)$$

$$= \frac{I_{Qw}\delta}{k_W} f_1(\xi) + \frac{q\delta^2}{2k_W} f_2(\xi) \,, \qquad (8a)$$

where

$$\xi = (1 + 2\delta/d)^2 \qquad (8b)$$

$$f_1(\xi) = \frac{\sqrt{\xi}\ \ln \xi}{2\,(\sqrt{\xi} - 1)} \qquad (8c)$$

$$f_2(\xi) = \frac{\xi \ln \xi - \xi + 1}{2(\sqrt{\xi} - 1)^2} \quad . \tag{8d}$$

Equations (8) describe the one-dimensional slab when $\xi \to 1$, the functions $f_1(\xi)$ and $f_2(\xi)$ giving the thick-walled-cylinder corrections.

Since both the maximum tube-wall temperature, T(0), and the associated bulk coolant temperature, T_c, are to be specified by the parametric analysis, the temperature change, ΔT_f, across the coolant boundary layer must be determined. This film drop at the coolant-tube exit is given by

$$\Delta T_f = T(\delta) - T_c$$

$$= I_w \left[(I_{Qw}/I_w)\,(1 + 2\delta/d)/\pi + (q/I_w)\delta(1 + \delta/d)\right]/h \tag{9}$$

The Dittus-Boelter correlation[18] is used to determine the film heat-transfer coefficient, h

$$\frac{hd}{k_c} = 0.023\ Re^{0.8}\ Pr^{0.4} \quad , \tag{10}$$

where $Re = u\rho_c d/\mu_c$ and $Pr = \mu_c c_p/k_c$.

For a pressurised-water coolant with sub-cooling $\Delta T_{SAT} = T_{SAT} - T_c$ the following expression is used to determine the coolant pressure.

$$P_c(\text{MPa}) = 2.59(10)^4 e^{-\,4635/(T_c + \Delta T_{SAT})} \quad . \tag{11}$$

Generally, both T_c and ΔT_{SAT} are specified, and P_c is then calculated to estimate the primary (pressure) stress. The primary stress for an internally pressurised thick-walled tube is given by

$$\sigma_p = P_c\ f_3(\xi) \tag{12a}$$

$$f_3(\xi) = \frac{\xi + 1}{\xi - 1} \quad . \tag{12b}$$

Similarly, the secondary thermal stress is given by

$$\sigma_{TH} = \frac{\alpha \, E \, \Delta T_w}{2 \, (1 - \nu)} \, f_4(\xi) \qquad (13a)$$

$$f_{4(\xi)} = 2 \, \frac{1 - (\ell n \, \xi)/(\xi - 1)}{\ell n \, \xi} \, , \qquad (13b)$$

where the coefficient of thermal expansion is α, Young's modulus is E, and Poisson's ratio is ν. Defining $M = 2(1 - \nu)k_w\sigma_Y/\alpha E$ as the thermal stress parameter, the total stress in a thick-walled coolant tube is given by

$$\frac{\sigma}{\sigma_Y} = \frac{P_c}{\sigma_Y} f_3(\xi) + \frac{k_w \, \Delta T_w}{M} f_4(\xi) \, . \qquad (14)$$

The temperature dependence of M for a range of alloys, including the base-case stainless steel and copper alloy considered herein, is depicted on fig.2.

Equation (14) gives the desired relationship between δ, d and I_w for given temperatures T(O) and T_c, physical properties, and normalised stress, σ/σ_Y. The functions $f_3(\xi)$ and $f_4(\xi)$ give the thick-walled-cylinder corrections. Typically, d is specified, and from the relationship between δ and I_w that results a measure of overall system performance is made parametrically. Equation (14) can be used in conjunction with equations (7) to establish other surfaces or regions on the I_{Qw} versus δ modified Bree diagram. Also, by specifying fatigue or creep strain, $\varepsilon_{TH} = \sigma_{TH}/E$, a limit established by fatigue or creep life, respectively, can be determined; typically ε_{TH} is set to 0.001 - 0.005, without relating to the specific number of burn cycles (fatigue) or time at pressure (creep). The integral results from a separate study[14] that examines the trade off between thermal cyclic fatigue and sputter erosion, however, are included.

One measure of system performance has already been suggested by equation (4) as the (derated) thermal efficiency. Another measure is the pump power required to drive the first wall coolant at Reynolds numbers that are sufficient to achieve the heat transfer coefficient required. Together, the decreased thermal conversion efficiency, η_{TH}, and increased recirculating power, ε, gives a first wall related degradation of the overall

plant efficiency, $\eta_p = \eta_{TH}(1 - \varepsilon)$, which in turn gives the trade off between increased specific capital cost (UDC) as I_{Qw} is increased and the generating cost (COE). The ratio of pumping loss incurred in a unit length of coolant tube to the total fusion power passing through and generated within that tube wall is given by

$$\varepsilon_p = \frac{\frac{\pi}{2}\rho_c \kappa_c^3 f_F Re^3/d^3}{I_w(M_N + \frac{1}{4})(1 + 2\delta/d)} , \qquad (15a)$$

where

$$f_F = 0.046/Re^{0.2} \qquad (15b)$$

is the Fanning friction factor and $\kappa_c = \mu_c/\rho_c$. The generic nature of this study relates ε_p and ε to a unit length of first wall; a detailed reactor design is required to assess exact trade offs related to first wall configuration, blanket thickness, lengths of coolant mains, degree of toroidal segmentation etc.

Lastly, some measure of critical heat flux (CHF) is desirable for high-performance, water-cooled systems. The Griffel CHF correlation[18] is used to monitor this important constraint.

$$CHF(MW/m^2) = [1.4\ (10)^{-8}\ Re/d + 1.42]\ [4.4 + \Delta T_{SAT}]^{0.27} \qquad (16)$$

Defining a pump efficiency, η_{pump}, equations (4) and (15) can be combined to give an expression for the decrease in plant efficiency, η_p, because of the added first wall coolant pumping power and reduced overall thermal efficiency associated with the high heat-flux first wall. If ε_o is the minimum recirculating power fraction for an idealised system operating with maximum thermal efficiency η^o_{TH} [i.e. $f_{FW} \simeq 0$ in equation (4)], the reduced plant efficiency relative to the maximum value, $\eta^o_p = \eta^o_{TH}\ (1 - \varepsilon_o)$ is given by

$$\frac{\eta^o_p - \eta_p}{\eta^o_p} = \frac{\Delta\eta_p}{\eta^o_p} = \frac{\eta'_{TH}}{\eta^o_{TH}} f_{FW} + \frac{\varepsilon_p}{\eta^o_{TH}\ \eta_{pump}(1 - \varepsilon_o)} . \qquad (17)$$

This expression describes the major penalties associated with high-heat-flux first walls related to a reduced overall plant efficiency because of: (a) a fraction f_{FW} of the fusion power being extracted through the first wall coolant circuit at a potentially lower temperature and, hence, reduced thermal efficiency, and (b) increasing pump power required to drive high velocity coolant through a first wall system that is constrained to operate within specific temperature and stress limits. These constraints reduce η_p as I_w is increased, until either costly and inefficient systems result, or the constraints must be relaxed.

The economic merits of high-power-density operation are contained primarily in the unit direct cost, which is reduced because of the lower fusion power core mass per unit power output and the increased system power density resulting from the increased wall loading. This merit must be included in the analysis in order to perform a trade-off study. A condensed costing model using the cost of electricity as a figure-of-merit with which to examine parametric sensitivities and trade offs is described for this purpose in the following section.

2.3 Economics and Costing Model

The costing model used in the STARFIRE tokamak reactor design[24], as constrained by the guidelines suggested in Reference 25, has been expressed in conveniently condensed analytic form[26]. A summation of all cost scaling laws given in Reference 26 results in an even simpler expression for the unit direct cost (UDC), which includes only the cost of fabricated and installed systems and associated contingency cost (15%) and spare parts allowances (3-4%). Interest and inflation during construction, construction facilities, equipment and services, engineering and construction management services and other costs are not included. For the conditions recommended in Reference 25 and used in Reference 26 these added costs would increase the total direct cost by a factor of 1.73 (assuming a 5-year construction time, a 10% interest rate and a 5% escalation rate). The simplified, analytic expression for the unit direct cost is given by

$$(1 - \varepsilon)\text{UDC} = F + \frac{C}{(P_{TH}/V_{FPC})} \tag{18a}$$

$$F \simeq \frac{538.2}{P_{ET}^{0.62}} + \frac{51.8}{\eta_{TH}} + \frac{16.6}{\eta_{TH}^{.8}\ P_{ET}^{.2}} \tag{18b}$$

$$C = \frac{1.17(10)^3\ c_{FPC}}{\eta_{TH}}\ , \tag{18c}$$

where $c_{FPC}(M\$/m^3)$ is the cost per unit volume of the fusion power core (FPC), ε is the recirculating power fraction, and $P_{ET}(GWe)$ is the gross electrical power output. Equations (18) show a fixed cost, that depends only on total plant capacity and thermal-conversion efficiency, and a cost component that depends on engineering volume and hence system power density, $P_{TH}/V_{FPC}(MWt/m^3)$.

In order that the simplified costing expression be useful in conjunction with the previously described first wall model, the FPC power density must be related to fusion neutron wall loading, $I_w(MW/m^2)$. This connection is made by noting that P_{TH}/V_{FPC} is related to I_w by the ratio of first wall area, A_{FW}, to the FPC volume, V_{FPC}. Specifically,

$$\frac{(P_{TH}/V_{FPC})}{I_w} = (M_N + \tfrac{1}{4})\ (\frac{A_{FW}}{V_{FPC}}) = \frac{M_N + \frac{1}{4}}{2\ (\Delta b + \Delta c)}\ \frac{4x}{(1 + x)^2} \tag{19}$$

where $x \equiv r_w/(\Delta b + \Delta c)$ and equation (19) maximises at $x = 1$. The recasting of the unit direct cost in terms of wall loading rather than power density, however, is independent of x if the FPC cost is re-expressed per unit first-wall area, $c_{FW}(M\$/m^2) = c_{FPC}(M\$/m^3)\ (V_{FPC}/A_{FW})$. With $P_E = P_{ET}(1 - \varepsilon)$ defined as the net electric power, using equation (19), and with the above definition of $c_{FW}(M\$/m^2)$, equation (18) becomes

$$\text{UDC}\ (\$/kWe) = \frac{538.2}{P_E^{0.62}\ (1 - \varepsilon)^{0.38}} + \frac{16.6}{\eta_{TH}^{.8}\ (1 - \varepsilon)^{.8}\ P_E^{0.2}} \tag{20}$$

$$+ \left[51.8 + \frac{1.17\ (10)^3\ c_{FW}}{(M_N + \frac{1}{4})I_w}\right]\ \frac{1}{\eta_p}$$

Hence, the primary means by which increased wall loading affects the plant economics through the UDC are displayed in equation (20) through η_{TH} [equation (4)], $\eta_p/\eta_{TH} = (1 - \varepsilon)$ [equation (17)], and I_w directly.

The influence of power density and wall loading on the cost of electricity (COE) can be determined only once a means is developed to account for the effect of I_w on the plant availability, as measured by the plant (or load) factor, p_f. The COE is simply the sum of annual operating and investment costs divided by the annual net electric energy generation. The cost of replacement first wall and blanket systems ($c_{FW/B/S}$ M\$/m^3), will appear as an annual operating cost. Other operating costs are generally[25] estimated as 2% of the total direct cost and added to the annual Return on Investment (ROI $\simeq$ 0.15)[25]. Hence, with a first wall, blanket and shield volume of $V_{FW/B/S}$ and a net electric power of P_E(MWe), the COE can be computed from the following expression.

$$\text{COE (mills/kWeh)} = \qquad (21)$$

$$\frac{c_{FW/B/S}\, V_{FW/B/S}(10)^6\, p_f(I_w/I_w\tau) + (\text{ROI} + 0.02)\, 1.76\, \text{TDC}}{8760\, p_f\, P_E}$$

where $I_w\tau$ is the first wall and blanket radiation damage lifetime and the factor 1.76 reflects the indirect costs mentioned earlier. If $f_{FW/B/S} = (\text{UDC})_{FW/B/S}/\text{UDC}$ is the fraction of the direct costs attributable to the first wall, blanket and shield and ROI = 0.15, then equation (21) becomes

$$\text{COE} = \frac{\text{UDC}}{8.76}\left[f_{FW/B/S}\,\frac{I_w}{I_w\tau} + \frac{0.30}{p_f}\right] . \qquad (22)$$

Typically, radiation lifetimes in the range 10-15 MWyr/m^2 are expected, and $f_{FW/B/S}$ ranges from 0.15 for STARFIRE[24] to 0.014 for the compact Reversed-Field-Pinch (RFP) reactor[26]. The first term in equation (22) is generally small compared with the second term containing the plant factor p_f. Nevertheless, the importance of the indirect costs is clear; for $p_f \simeq 0.75$ the annual revenues generated by the plant must repay over 40% of the total initial direct capital cost.

The model for p_f suggested in Reference 26 is used. This model was adopted from the STARFIRE design, wherein 60 days/year are allotted for unscheduled maintenance, 28 days/year for scheduled maintenance, as long as such maintenance does not occur more than once a year; 28 P_f $(I_w/I_w\tau)$ days/year is required if more than one scheduled annual replacement is required because of high wall loadings and shortened chronological life. The following expression gives this dependence of p_f on I_w

$$p_f = \begin{cases} 0.76 & \text{if } I_w/I_w\tau < 1.32 \text{ yr}^{-1} \\ \dfrac{0.835}{1 + 0.0767\ (I_w/I_w\tau)} & \text{if } I_w/I_w\tau > 1.32 \text{ yr}^{-1} \end{cases} \qquad (23)$$

Hence, in addition to the costs and benefits incorporated into the capital cost, the generating cost (COE) can rise with increasing wall loading because of higher operational (replacement) costs and reduced plant factor.

Equation (20) for the unit direct cost and equation (22) for the cost of electricity must be used carefully to ensure that these highly condensed expressions are not applied beyond the intended range of validity. A comparison and calibration with existing tokamak and compact reactor designs is given. Once P_E, η_{TH}, and ε are determined, the key fixed parameters become the unit cost of the fusion power core and the fraction, $f_{FW/B/S}$, of the direct cost taken by the first wall, blanket and shield. Depending on whether power density or wall loading is used as the parametric variable, the FPC cost can be expressed in terms of $c_{FPC}(M\$/m^3)$ or $c_{FW}(M\$/m^2)$, the latter being used when the cost model is joined with the first wall thermal-mechanical model to evaluate the effects of high-power-density operation on COE. Most materials are or will be purchased on a unit mass basis, $c_{FPC}(\$/kg)$, however, rather than on an area or volumetric basis. Knowledge of the average or "smear" density of the FPC, ρ_{FPC}, is necessary to relate these various unit costs through the following relationships.

$$c_{FPC}\ (\$/kg) = \frac{10^6}{\rho_{FPC}}\, c_{FPC}(M\$/m^3)$$

$$= \frac{10^6}{\rho_{FPC}} \frac{A_{FW}}{V_{FPC}}\, c_{FW}(M\$/m^2)\ . \qquad (24)$$

In order to develop quantitative insight into the magnitude of ρ_{FPC} and the associated FPC unit costs being projected for the more recent fusion reactor designs, fig.3 is a plot of the FPC power density against inverse mass utilisation, and Table II gives a FPC performance comparison for two major tokamak reactor designs[24,27] and a recent design of a compact RFP reactor[19] (CRFPR). Also included on Table II are results from the more recent Mirror Advanced Reactor Study (MARS)[28]. Generally, when equation (21) is used to compare various reactor options, particularly compact versus more conventional options, the respective differences in the cost quantities, as reflected in Table II, must be taken into account.

It should be noted that even though the unit cost ($/kg) for STARFIRE (and MARS) is almost half that assumed for the CRFPR the cost per unit wall area of STARFIRE is a factor of 1.8 more than the CRFPR (2.7 for MARS). These superconducting systems (i.e. STARFIRE and MARS) require more high-technology mass behind each square metre of first wall, and even if that mass only costs half as much on a unit cost basis, its total cost will be more than for the compact systems.

The dependence of COE on I_w is shown in fig.4 for STARFIRE and CRFPR. The respective design points are also shown in fig.4. The fusion power core unit cost listed in Table II for STARFIRE and MARS amounts to ~ 20 $/kg, compared to ~ 40 $/kg assumed in the CRFPR study. Application of the latter unit cost to STARFIRE, along with a proportionate increase in $f_{FW/B/S}$, gives the "cost adjusted" STARFIRE curve in fig.4, which also includes a STARFIRE cost curve using the Reference 24 costs. The cost advantages of increased system power density and wall loading in either case is apparent from fig.4. The physics (beta, safety factor) and mechanical (coil peak fields and stresses) constraints for STARFIRE, however, will not allow access to the higher wall loading, lower cost design points while simultaneously maintaining the same net electric power output for this superconducting system.

The difficulties in both plasma and magnet performance encountered when attempting to access higher values of I_w and P_{TH}/V_{FPC} for otherwise constant-power STARFIRE-like systems are

best illustrated by an example. Since the net electrical power is given by $P_E = (2\pi)^2 (M_N + \frac{1}{4}) \eta_p A I_w r_w^2$ (see Table II for typical parameters), an increase from 3.6 MW/m^2 for STARFIRE to (say) 20 MW/m^2 requires r_w to be decreased from 2.83 m to 1.20 m, keeping $A = R_T/r_w$ and P_E constant. Since the blanket and shield thickness cannot be decreased (actually, it must be increased somewhat to maintain the same radiation and heat flux at the super-conducting magnets), the STARFIRE design moves even further from the optimum power density as $x = r_w/(\Delta b + \Delta c)$ decreases from 0.69 to 0.29 [$x = 1$ maximises $(P_{TH}/V_{FPC})/I_w$ or A_{FW}/V_{FPC} for a fixed M_N, equation (19)]. Since $I_w \propto (\beta B^2)^2 r_w$ and $I_w r_w^2$ is held constant, then $\beta B^2 \propto I_w^{3/4}$. Hence, for the same field on axis, presuming the coils are ready at a peak field of 11-12 T, the $\beta \propto I_w^{3/4}$ scaling dictates that beta would have to increase by a factor of 3.62 to 0.24, compared to the design value of 0.067; for any realistic pressure profile, an average beta of $\sim$ 0.24 would mean a beta of nearly unity on axis. Nevertheless, given that such improved plasma performance were possible, the system power density would be increased by at most in proportion to $I_w\, x/(1 + x)^2$ which gives a factor of 3.9, leading to a value of 2.0 MW/m^3 for STARFIRE. More significant increases in system power density are achievable by reducing, $(\Delta b + \Delta c)$, pointing towards further improvement by confinement systems that can operate efficiently (i.e. $\varepsilon \leqslant 0.15$-$0.20$) with normal copper magnets.

The COE versus I_w plots in fig.4 show a shallow minimum for the lifetimes ($I_w \tau$ = 15 MWyr/m^2) assumed. Figure 4 also gives the dependence of COE versus I_w on the assumed blanket lifetime. The COE shows a minimum at a value of I_w that will generally assure at least a year of reactor operation before blanket replacement is necessary. This behaviour depends strongly on the plant-factor algorithm [equation (23)] and is an area where more detailed work is needed.

2.4 Computational Algorithm

This section describes the procedure used to solve equations (1) - (22). The primary input variables are the first wall tube material and its peak temperature T(0). A 20% cold-worked 316 stainless steel and an AMAX-MZC copper alloy are selected as

representatives of two extremes: poor heat transfer but mechanically strong versus good heat transfer but mechanically not as strong at temperature. The material properties for copper[4,29] and stainless steel[30] are also summarised in Table I. The coolant outlet temperature T_c and sub-cooling ΔT_{SAT} are then specified, from which the coolant pressure is determined [equation (11)]. The thermophysical properties of the coolant are strongly affected by temperature and pressure and are calculated from analytic fits (accurate to $\leq$ 1% in the range of interest) to data in steam tables[31], only nominal values being given in Table I.

The tube inner diameter, d, and stress constraint are then specified, enabling the thermomechanical model to be solved as a function of the surface heat loading, I_{Qw}. Equations (8) and (14) are solved simultaneously for the tube wall thickness, δ, and the temperature drop through the wall ΔT_w. The film temperature drop, ΔT_f, and, therefore, the Reynolds number, Re, are then determined, from which follow the frictional pressure drop and the degradation in plant efficiency related to recirculating power consumed by the coolant pumps. Finally, the net power output P_E, wall lifetime $I_w\tau$, and the first wall blanket and shield cost ratio $f_{FW/B/S}$ are specified, and the UDC and COE are calculated. The thermal-mechanical results are displayed as plots of I_{Qw} versus δ with stress limits, T(O), T_c, and d being varied for each material. The cost results are shown as curves of COE versus neutron wall loading I_w. For all cases the connection between surface heat flux, I_{Qw}, and I_w is made by assuming the worst case for the first wall when $f_L = 0$ [equation (1), i.e., no divertor].

3. RESULTS

3.1 Base-Case Operation

The base-case values used for the major parameters of the model are shown in Table III. Generally, these parameters are held fixed throughout this study and are typical of the reactor designs summarised in Table II.

Figure 5 compares stainless steel and copper-alloy first walls on a plot of surface heat load I_{Qw} versus wall thickness δ in the form of a modified Bree diagram. Also shown are lines representing a pumping power fraction, ε_p, of 0.3 (corresponding to a recirculating power fraction, ε, of approximately unity) and the minimum wall thickness needed to satisfy the time-independent primary stress limit, S_m, as given by the ASME code[20]. The ASME code criterion adopted equated the maximum allowable stress to the lower of $(1/3)\sigma_u$, and $(2/3)\sigma_Y$ (for copper) or $0.9\ \sigma_Y$ (for stainless steel). As both the copper-alloy and stainless steel materials considered here undergo substantial cold-working in order to attain their optimum mechanical properties, the ratio of yield stress to ultimate tensile strength approaches unity. The limit of $(1/3)\sigma_u$, therefore, provides the stronger constraint on time-independent stress levels.

To satisfy these constraints on pumping power and primary stress a first wall tube assembly would have to be operated below the line of constant ε_p on fig.5 and to the right of the $\sigma_p = S_m$ line. It is apparent from fig.5 that even these minimum constraints will restrict operation to the elastic regions below the $\sigma/\sigma_y = 1$ curve for both materials. This conclusion was also reached in another study[14] and can be explained by noting the high ratio of yield stress to ultimate tensile strength. Subsequent plots of this form will therefore be simplified by showing the curves of constant σ/σ_y and omitting the curves from the modified Bree diagram delineating the plastic, shakedown and ratchetting regimes.

Figure 6 repeats fig.5 after the Bree lines are eliminated, but with the addition of extra lines of constant pumping power ratio, constant secondary strain, ε_{TH}, and constant safety margin on critical heat flux (CHF/I_{Qw}). Rigid limits on these three

parameters do not exist, but typical values can be suggested. A limit on ε_p might be of the order of 1%, recalling that this ratio is based on the total thermal power output and not just that fraction removed by the first wall. For a pumping efficiency of η_{pump} = 75% and η_{TH} = 0.35, ε_p of 1% corresponds to a recirculating power fraction (due to the first wall coolant pumping power only) of ε = 3.8%. The maximum allowable cyclic strain depends on the number of cycles required by a specific design; a conservative upper limit for $\sim 10^5$ cycles typically would require $\varepsilon_{TH} \leq 0.1\%$ for either material. A safety factor of 2 on critical heat flux should be sufficient to prevent burnout resulting from local non-uniform heating and to give some margin for abnormal conditions. To operate within these limits requires a point on fig.6 to be below the curves of constant ε_p and ε_{TH} and to the right of the constant CHF/I_{Qw} curves. Together with the minimum wall thickness imposed by the primary stress limit, $\sigma_p = S_m$, these constraints restrict operation to a window in the thicker-wall, lower-heat-loading regions. The boundary of the design window for each material, subject to the constraints $\sigma_p < S_m$, $\varepsilon_p \leq 0.01$, $\varepsilon_{TH} \leq 0.1\%$ and $CHF/I_{Qw} \geq 2$, is shown in fig.6 by a thicker line. It is emphasised that these operating windows are not rigid, but are subject to some diffusiveness dependent upon modelistic assumptions and fixed parameters; the sensitivity of the operating window to parameter variations is examined later.

For the copper-alloy case at the base operating conditions (Table III) the critical heat flux limit eliminates a small section of the domain mapped out by the pumping power and primary stress limits. A narrow strip permitting operation at a surface heat loading up to 8 - 9 MW/m^2 and a wall thickness of $\sim$ 0.8 - 0.9 mm exists, but this strip is very sensitive to the precise values of temperature and tube diameter.. The constraints on CHF and cyclic strain for stainless steel provide the upper limit on heat flux of approximately 2 MW/m^2. In this case, owing to the relatively poor thermal conductivity of stainless steel, the restriction on thermal strain places a more severe limit on heat flux than the restriction on pumping power.

Another consideration in determining allowable wall thicknesses, although not addressed explicitly in this study, is erosion of the first wall caused by sputtering. Although divertors may alleviate this problem, erosion rates are likely to be significant and an allowance of ~ 1 mm/year is commonly suggested. First wall chronological lifetimes greater than year are generally required to give acceptably high plant factors (see section 2.2) and acceptably low component replacement costs. This requirement in itself suggests $\delta \geq 2$ mm will be necessary and that thicker walls (within limits imposed by requirements for ε_p and ε_{TH}) are favoured. However, a further restriction is that a thick wall can result in a significant fraction of neutrons being parasitically absorbed in the first wall. The necessity of achieving a tritium breeding ratio in excess of unity may place an upper limit on first wall thickness, but this limit is expected to be significantly greater than the lower limit suggested above[19].

The combined influences of thermal creep, cyclic thermal fatigue and sputter erosion have been examined using an iteration scheme that assures equal creep-fatigue and erosion lifetime[14]. The model incorporated the thin-wall approximation and neglected volumetric heat generation in calculating temperature profiles and thermal stresses. Only copper alloy was considered in the Reference 14 calculations, in which a 20 minute burn and an erosion rate of 1 mm/yr were assumed. Figure 7 compares the results of this creep/fatigue/erosion constrained calculation for the base-case conditions (Table III) and ε_p = 0.01 with the copper alloy results from this paper.

The two sets of calculations show similar trends, but the Reference 14 results give a higher heat flux at a given wall thickness. This is because the constraint on peak temperature (350°C for the base-case in this paper) has been lifted, allowing it to float to a higher value (typically ~ 390°C) in order to impose the extra constraint on equalising the creep-fatigue and erosion lifetimes. The Reference 14 results illustrate the very limited erosion lifetime available at high wall loadings although it is interesting to note that the product of neutron wall loading I_w (assuming $f_L = 0$) and creep/fatigue/erosion lifetime

for these conditions exceeds 15 MWyr/m^2 (the base-case value of radiation damage lifetime) for all $I_w \leq 50$ MW/m^2.

The combined results of figs. 6 and 7 suggest that a "realistic" wall thickness of ~ 2-3 mm (to give a chronological wall lifetime of ~ 1-2 years) will limit heat fluxes to ~ 0.6-0.8 MW/m^2 for stainless steel and to ~ 3.5-5 MW/m^2 for copper alloy, the limiting constraints being cyclic strain and pump power respectively. Furthermore, the pumping power constraint for the copper first wall is not a hard limit, being highly design sensitive and probably allowing even higher flux limits to be applied to a practical design.

3.2 Cost Variations

The influence of the thermal-mechanical model on global cost is now addressed, the values assumed for the cost-relevant parameters being given in Table IV. The first wall affects the cost of electricity through the neutron wall loading, I_w, which influences the unit direct cost and the plant factor, and also through its influences on the net plant efficiency via the parameters T_c, ε_p, and f_{FW}. The coolant exit temperature, T_c, is held fixed, the thermal efficiency varying by only 2 percentage points as T_c changes from 215 to 315°C [equation (4)]. The fraction f_{FW} of the total thermal power deposited into the first wall depends on the constant surface heat load and the volumetric heating in the tube wall, which also is a second-order effect. The only first wall variable that strongly influences the generating cost for fixed σ/σ_y is ε_p. Furthermore, to affect significantly the net plant efficiency, ε_p must be large, [of order ~ 0.1, equation (17)]. The cost of electricity, therefore, is expected to be virtually independent of the first wall conditions until ε_p reaches a sufficiently large value, at which point the COE will begin to increase rapidly, this point depending on T(0) and hence on the material.

Figure 8 plots the relative generating cost ($\propto$ COE) as a function of I_w for each material for various values of ε_p to illustrate this pattern. The upper limit on I_w is imposed by the primary stress constraint (see fig.6); limits due to the constraints on critical heat flux and thermal strain are not

included on figure 8.

For low values of ε_p (less than about 0.01) the generating cost is determined by I_w and the cost-relevant parameters given in Table IV; the cost of electricity in this region is essentially unaffected by the first wall conditions or the tube wall material. As ε_p is increased above 0.01 the cost rises rapidly for each material; in such regions of high ε_p, design changes would be made that would allow previously fixed parameters to be reoptimised; illumination of such design choices, of course, is beyond the scope of this generic, parametric study.

An alternative approach would be to specify an upper limit on ε_p as a constraint to eliminate the high-ε_p regime and specific design choices from consideration, effectively decoupling the first wall from cost except via the choice of I_w. Such a limit was suggested, somewhat arbitrarily, in the previous section on the grounds of what seemed a "reasonable" recirculating power. The connection with relative generating costs now allows a limit on ε_p to be imposed from the more practical viewpoint of its effect on the plant economics. Figure 8 shows that for $\varepsilon_p = 0.01$ (the limit recommended earlier) the cost of electricity is typically 2.5% higher than its limiting value as $\varepsilon_p \to 0$. At higher pumping powers the generating cost increases rapidly and for lower values of ε_p the primary stress limit begins to reduce the attainable wall loading sharply, particularly for copper alloy. The selection of 1% as an upper limit on ε_p is thus justified on economic as well as intuitive grounds.

None of the other constraints on primary stress, cyclic strain, and critical heat flux influences the cost directly, although these constraints should be carefully chosen to ensure that the creep or fatigue (or sputtering erosion) lifetime is not significantly different from the radiation damage lifetime, $I_w\tau$.

Figure 9 is another plot of relative generating cost versus I_w for each material; these curves give the cost of electricity at all points on the boundary of the design window (shown by a thicker line in fig.6). There are two points on this boundary

for any value of I_w (or I_{Qw}) owing to the nature of the constraints determining the boundary. The COE corresponding to any point within the design window of fig.6 for either material lies within the two branches of the corresponding curve in fig.9. The assertion that selecting a low limit for ε_p decouples the first wall from cost is well demonstrated in fig.9 as the two branches of the COE curve for each material lie extremely close to each other. The two sides of the curve are virtually superimposed for the stainless steel case as the constraint on ε_{TH} restricts ε_p to an even lower value than the upper limit of 1%.

The overall result from the cost model is a universal curve of COE as a function of neutron wall loading that is independent of the first wall conditions and is determined by such parameters as power output and radiation damage lifetime (as in fig.4). Adjusting the values of parameters relevant to the first wall (i.e. T(0), T_c etc) will allow access to different portions of this universal COE versus I_w curve, but will not define new operating regions. The selection of a low limit on pumping power (e.g. $\varepsilon_p = 0.01$) and the use of other constraints that ensure the creep-fatigue lifetime is not shorter than the radiation damage lifetime allows the questions of the first wall and global cost to be addressed separately, with cost always being related to first wall conditions through the universal COE versus I_w curve. The extent to which variation of the thermal-mechanical parameters permits access to different wall loadings is now examined.

3.3 Sensitivity Studies

With the decoupling of the economic figure-of-merit (COE) from the base-case operating parameter variations, the sensitivity of the I_{Qw}-δ operating window (fig.6) to parameter changes can now be examined with a less direct reference to the universal cost curves (fig.8 and 9).

Figure 10 shows the effect of varying the peak wall temperature T(0) while holding the values of the other parameters constant. The only constraints plotted are $\varepsilon_p = 0.01$, $\varepsilon_{TH} = 0.1\%$, $CHF/I_{QW} = 2$, $\sigma/\sigma_y = 0.3$, and the primary stress limit ($\sigma_p = S_m$).

The temperatures investigated are specific for each material; the lower temperature results (325°C for copper alloy, 400°C for stainless steel) are shown as full lines, the higher temperature results (400°C for copper, 500°C for steel) as broken lines. The intermediate case for each material is shown in fig.6.

As the material properties change only slightly with temperature, the boundaries set by primary-stress and σ/σ_y constraints are largely unaffected. Creep at higher temperatures, however, can reduce the primary stress limit from its time independent value, $\sigma_p = S_m$, and would be included explicitly in a deeper study. The thermal strain is determined by I_{Qw} and the material properties so the curve at constant ε_{TH} remains almost stationary for changes in any of the first wall parameters. At the lower temperatures, the film temperature drop is reduced as T_c is maintained fixed, which leads to a requirement for a higher heat-transfer coefficient. The resulting higher values of the Reynolds number yield a higher pumping power and also a higher value of CHF; the $CHF/I_{QW} = 2$ curve does not appear on the plot at the lower temperature for each material. For copper at thicknesses of prime interest (~ 2 - 3 mm), the attainable heat loading is limited by pumping power at low temperatures and CHF at higher temperatures; neither temperature allows a higher I_{Qw} than the intermediate case given in fig.6. For stainless steel, the cyclic strain is the dominant limit at all temperatures.

The effect of varying the coolant outlet temperature, T_c, at the base-case material temperatures is displayed in fig.11. Reducing T_c (with constant sub-cooling) lowers the coolant pressure and expands the accessible region governed by stress constraints. This improved access, however, occurs in the unfavoured region of thin walls. A further result of lower T_c is a reduced CHF, which now impacts the design more strongly, particularly for the copper case shown in fig.11. As in the T(O) variation (fig.10), a high T_c leads to higher pumping powers and the trade-off between the CHF and ε_p constraints again suggests that the highest heat fluxes are attainable for the base-case values of T(O) and T_c. Cyclic strain again provides the limit on stainless steel throughout.

A narrow-bore tube also allows thinner walls and higher heat fluxes to be used from the stress aspect, as shown in fig.12. The CHF problem is slightly increased at low d, but the pumping power is not changed greatly. No significant improvement in I_{Qw} is found as d is changed for δ of the order of 2 mm.

Exposure of a copper first wall to the fusion neutron spectrum will transform the alloy over the exposure period as nuclear transmutation products accumulate. The major transmutation products are nickel and zinc and to a lesser extent, cobalt. These new alloying constituents change the electrical, thermal, and mechanical properties. The increased electrical resistivity[32] for additions of nickel to copper amounts to $\rho/\rho_o \simeq 1 + 0.8\ f_{Ni}$ for $f_{Ni} \leq 20$ wt %. The effectiveness of zinc in increasing ρ is 0.32 times that of nickel (i.e., $\rho/\rho_o \simeq 1 + 0.26\ f_{Zn}$). Nickel and zinc build into pure copper at rates of 0.24 and 0.13 wt % per year respectively for each unit of neutron wall loading, $I_w(MW/m^2)$[19,33]. Although the effectiveness of cobalt in increasing pure-copper resistivity is 5.2 times that of nickel, cobalt is generated at only 4% of the nickel rate and, therefore, is ignored as a contribution to resistivity increase. Taking the upper value for the nickel/zinc generation rate and weighting in accordance to the relative effect on resistivity increase gives the following approximate expression for ρ as a function of $I_w(MW/m^2)$ and exposure time, τ(yr).

$$\rho \simeq \rho_o\ [1 + 0.23\ I_w\tau] \qquad (25)$$

The Weidemann-Franz law[34], (i.e., $\rho k_w/T \simeq 2.5\ (10)^{-8}$ W ohm/K^2) can be used to relate the increased resistivity, ρ, to the decreased thermal conductivity. Hence,

$$k_w = k_o/[1 + 0.23\ I_w\tau] \qquad (26)$$

For the base-case value of $I_w\tau = 15$ MWyr/m^2, a decrease in k_w by as much as a factor of four may be possible, this value representing an upper value depending on whether the transmutation products add to the crystal matrix, are incorporated at grain boundaries, or

form a second phase.

The direct result of a lower value of k_w is a higher temperature drop through the tube-wall, leading to increased thermal stresses and cyclic strain. The lower film temperature drop [equation (9)] requires higher pumping powers but reduces the importance of CHF limits. The effect of degraded thermal conductivity for the copper-alloy base-case (fig.6) are shown on fig.13. The value of the coefficient in equation [26] was reduced from 0.23 to 0.13 to account approximately for the grain boundary effects mentioned earlier to obtain these results. For first wall thicknesses between 2 and 3 mm the maximum heat flux falls by a factor of ~ 2.5 to 1.3 - 2 MW/m^2, with cyclic strain now providing a slightly more severe constraint than pumping power. Even these reduced, end-of-life heat fluxes, however, are a factor of 2 - 3 higher than the maximum values permitted for stainless steel (fig.6).

4. CONCLUSIONS

The interactions of the thermal-mechanical performances of the first wall of a fusion reactor with the overall plant economics have been investigated with the aim of assessing the merits and demerits of high power density fusion systems. A model of a water-cooled tube-array first wall and a condensed costing model normalised to recent reactor studies have been used. In addition to the magnitude of the neutron wall loading and the wall lifetime, the first wall influences the overall cost via the reduced temperature at which heat is removed from the first wall system and via the coolant pumping power, both effects leading to a reduced overall plant efficiency and increased cost.

The first wall system affects the generating cost through the plant efficiency. Imposing realistic limits on coolant pumping power (~ 1% of total thermal power output), however, results in the plant efficiency and hence the cost of electricity being largely independent of the first wall conditions for a given neutron loading. Provided that the first wall is not operated in regimes such that its creep, fatigue, or sputtering erosion lifetime is less than the radiation damage lifetime then the two issues of the first wall and global cost can be

considered separately. Adjusting the first wall operating variables may allow access to different regions of the universal cost of electricity versus neutron wall loading curve by increasing the allowable heat flux, but new regions will not be defined. The radiation damage lifetime is thus identified as a crucial parameter and an investigation of the various life-limiting processes is required in order to optimise the wall loading. Upon determination of the "universal" cost curves (generating cost versus wall loading I_w) for the two alloys considered (MZC copper and 316 stainless steel), the relative merits of a high heat flux/low strength alloy compared to a low heat flux/high strength alloy can be assessed in terms of thermal-mechanical boundaries in a surface heat flux I_{Qw} versus wall thickness δ phase space.

Trade studies were performed that examined the sensitivity of the maximum allowable heat flux to changes in stress (expressed as a fraction of yield), strain (fatigue), critical heat flux (CHF), recirculating (pumping) power, peak material temperature, coolant exit temperature (and coolant pressure for a given degree of sub-cooling), coolant-tube diameter and wall thickness, and radiation-induced changes in thermal conductivity (for copper only). Elastic, plastic and ratchetting limits were also examined, these constraints generally being less restrictive than those imposed by creep, fatigue, CHF, and pumping power for both the stainless-steel and copper alloys, owing to the high ratio of yield stress to ultimate tensile strength obtained by substantial amounts of cold-working. A similar behaviour is indicated for creep, fatigue and sputter-erosion limits established from other studies for the copper alloy first wall.

For the typical base-case values (Table III) assumed, the copper alloy allows significantly higher surface heat fluxes ($I_{Qw} \simeq 3\text{-}5$ MW/m^2) than for stainless steel ($I_{Qw} \simeq 0.3 - 0.5$ MW/m^2), which when related to the universal curves of cost of electricity indicates a potential for higher first-wall loadings and a lower cost system; these indications are based on a generic fusion system in which $I_{Qw} \simeq I_w/4$ (i.e., no divertor, uniformly irradiated first wall). For the copper alloy the limiting constraints are usually the coolant pumping power (for a given

coolant temperature and peak material temperature) or the CHF; generally increasing the difference between these two temperatures lessens the importance of the pumping power constraint but makes the CHF constraint more restrictive. For the stainless steel alloy the cyclic strain (fatigue) represents the major limit, along with creep and, in certain cases, the CHF.

Although a superior performance is predicted for a copper-alloy first wall, the materials properties data base requires considerable expansion before this promise can be realised. Fatigue, creep, alloy changes, and sputter erosion in an intense radiation field remain to be documented, particularly as they degrade thermal-mechanical performance and lifetime of the first wall. Specific first wall designs are required to assess more accurately the coolant pumping power requirement, as well as fabrication and joining methods. Degradation of the thermal conductivity and changing mechanical properties of the copper alloy exposed to large neutron fluences remains to be determined, although information on the effects of transmutation products on the thermal and mechanical properties of copper and copper alloys will be soon forthcoming[35]. Nevertheless the copper alloy appears to offer access to higher power density fusion approaches, with a potential for improved system economics and power-plant operations[1].

5. REFERENCES

1. R.A. Krakowski and R.L. Hagenson, "Compact Fusion Reactors", 5th ANS Topical Meeting on the Technology of Fusion Energy, Knoxville, TN (April 26-28, 1983), Nucl. Technology/Fusion 4, 1265 (1983).

2. S.O. Dean, "Implications of Compact Fusion Concepts and their Relationship with the Federal Program", a workshop organised for the NSF by Fusion Power Associates, San Diego, CA (September 30 - October 1, 1982).

3. G.E. Cort, A.L. Graham and K.E. Christensen, "A High-Flux First-Wall Design for a Small Reversed-Field Pinch Reactor", AIAA/ASME Conf. on Fluid, Plasma, Thermophysics and Heat Transfer, St Louis, MO (June 8-11, 1982).

4. A. Caie and G.J. Butterworth, "The Design of a 316 Stainless Steel First Wall for a Pulsed Fusion Reactor with Wall Loading Greater than 10 MW/m^2", Proc. Symp. on Fusion Technology, Julich, September 1982 2 845-850 (1982).

5. R.W. Conn, "Magnetic Fusion Reactors", Fusion Vol.I., E. Teller (ed) pp 281-287.

6. C.K. Youngdahl and D.L. Smith, "Stress and Lifetime Limitations of First-Wall Structural Materials", J. Nucl. Mater. 85 and 86, 153 - 157 (1979).

7. A.O. Adegbulugbe and J.E. Meyer, "Failure Criteria for Fusion Reactor First Wall Structural Design", Proc. 2nd Topical Meeting on Fusion Reactor Materials, Seattle, WA (August 9 - 12, 1981), J. Nucl. Mater. 103, and 104, 161-165 (1982).

8. M.A. Hoffman, R.W. Werner, T.R. Roose and G.A. Carlson, "Fusion Reactor First-Wall Cooling for Very High Energy Fluxes", Nucl. Eng. Design 36, 37-46 (1976).

9. M.A. Hoffman, "Heat Flux Capabilities of First Wall Tube Arrays for an Experimental Fusion Reactor", Nucl. Eng. Design 64, 283-299 (1981).

10. P.J. Gierszewski, B. Mikic, N.E. Todreas, "Design Limit Analysis of Redundant Tube Array First Walls", Massachusetts Institute of Technology report PFC/RR-82-32 (December 1982).

11. R.F. Mattas, "Fusion Component Lifetime Analysis", Argonne National Laboratory report ANL/FPP/TM-160 (September, 1982).

12. R. Matera, C. Ponti, R. Van Heusden, M. Biggio, A. Perfumo, "SMILE - A Computer Program for Evaluating the Lifetime of Fusion Reactor Structural Components", Nucl. Eng. Design/Fusion 1, 127-136 (1984).

13. D.L. Smith et al, "Fusion Reactor Blanket/Shield Design Study", Argonne National Laboratory report ANL/FPP-79-1 (July, 1979).

14. A. Caie and G.J. Butterworth, "A Study of the use of a High Strength Copper-Alloy for the First Wall of a High Heat Flux Fusion Reactor", Culham Laboratory Report (to be published, 1984).

15. J.N. Goodier, "Thermal Stress in Long Cylindrical Shell due to Temperature Variation Round the Circumference and through the Wall", Canadian J. Res. 4, 15 (1937).

16. C.H. Tsao, "Thermal Stress in Long Cylindrical Shells" J. Appl. Mechanics 26, 147, (1959).

17. D.R. Cohn et al, "High Field Compact Tokamak Reactor (HFCTR) Conceptual Design", MIT Fusion Centre report RR-79-2 (January, 1979).

18. W.H. Rohsenow, "Boiling", Handbook of Heat Transfer, W.H. Rohsenow and J.P. Hartnett (ed), Section 13, ppl3.34 - 13.63, McGraw-Hill, NY (1973).

19. R.A. Krakowski, R.L. Hagenson, C.G. Bathke, R.L. Miller, M. Embrecht, N.M. Schnurr, M.E. Battat and R.J. La Bauve, "Compact Reversed-Field Pinch Reactors (CRFPR): Preliminary Engineering Considerations", Los Alamos National Laboratory Report (to be published, 1984).

20. ASME Boiler and Pressure Vessel Code, Case N-47-21, Class 1 Components in Elevated Temperature Service, Section III, Division 1, Approved December 11, 1981.

21. J. Bree, "Elastic-Plastic Behaviour of Thin Tubes subjected to External Pressure and Intermittent High-Heat Fluxes with Application to Fast Nuclear-Reactor Fuel Elements", J. Strain Analysis 2 (3), 226 (1967).

22. W. O'Donnell and J. Porowski, "Upper Bounds for Accumulated Strains Due to Creep Ratchetting", Trans. ASME, J. of Pressure Vessel Technology, 96, 126 (1974).

23. T. Bui-Quoc and A. Biron, "A Phenomenological Approach for the Analysis of Combined Fatigue and Creep", Nucl. Eng. and Design 71, 89-102 (1982).

24. C.C. Baker et al, "STARFIRE - A Commercial Tokamak Fusion Power Plant Study", Argonne National Laboratory report ANL/FPP-80-1, (September 1980).

25. S.C. Schulte, W.E. Bickford, C.E. Willingham, S.K. Ghose and M.G. Walker, "Fusion Reactor Design Studies - Standard Costs and Cost Scaling Rules", Pacific Northwest Laboratory Report PNL-2987 (September 1979).

26. R.L. Hagenson and R.A. Krakowski, "Compact Reversed Field Pinch Reactors (CRFPR): Sensitivity Study and Design - Point Determination", Los Alamos National Laboratory report LA-9389-MS (July 1982).

27. A.A. Hollis, "An Analysis of the Estimated Capital Cost of a

Fusion Reactor", UKAEA Harwell report AERE-R 9933 (June 1981).

28. B.G. Logan, "The Mirror Advanced Reactor Study (MARS)", Nucl. Tech/Fus. 4, 563 (1983).

29. C.C. Baker et al, "STARFIRE", Appendix E.

30. J.W. Davis and G.L. Kulcinski, "Assessment of Titanium for use in the First Wall and Blanket Structure of Fusion Power Reactors", Electric Power Research Institute Report EPRI-ER-386 (April 1977).

31. "UK Steam Tables in SI Units 1970", published for UK Committee on the Properties of Steam by E. Arnold Ltd (1970).

32. R.M. Brick, A.W. Pense, R.B. Gordon, Structure and Properties of Engineering Materials, McGraw-Hill Book Co., N.Y. (1977) p.66.

33. R.L. Hagenson, R.A. Krakowski and C.F. Cort, "The Reversed-Field Pinch Reactor (RFPR) Concept", Los Alamos National Laboratory report LA-7973-MS (August 1979).

34. C. Kittel, Introduction to Solid State Physics, John Wiley and Sons, Inc. N.Y. 4th Ed. (1968) p.221.

35. F. Clinard, Jr., Los Alamos National Laboratory, personal communication (1984)

36. C.G. Bathke et al, "ELMO Bumpy Torus Reactor and Power Plant Conceptual Design Study", LA-8882-MS, Los Alamos National Laboratory (August 1981)

37. R.I. Miller, C.G. Bathke, R.A. Krakowski et al, "The Modular Stellarator Reactor: A Fusion Power Plant", Los Alamos National Laboratory report LA-9737-MS (July 1983)

38. A Technical Outline of Sizewell 'B': The British Pressurised Water Reactor" UK Central Electricity Generating Board (1983).

39. R.F. Bourque, "OHTE Reactor Embodiments Based on Preliminary RFP Experimental Results" 5th Top. Mtg. on the Tech. of Fus. Energy, Knoxville, TN (April 26-28, 1983).

40. R. Hancox, R.A. Krakowski and W.R. Spears, "The Reversed Field Pinch Reactor (RFPR) Concept", Nucl. Eng. and Design 63, 251 (1981).

41. R.W. Bussard and R.A. Shanny, "Conceptual Design of a Modular Throwaway Tokamak Commercial Fusion Power Plant", Internal report, INESCO Inc., 27 April 1978, see also C.A. Robinson, "Aerospace Aids for Fusion Power Concept", Aviat. Week and Space Technol. 108 61 (12 June 1978).

42. C.E. Wagner, "Possibility of Achieving Ignition in a High-Field Ohmically-heated Tokamak", Phys. Rev. Lett 46, 654 (1981).

43. J.T.D. Mitchell, "Blanket Replacement in Toroidal Fusion Reactors", Proc. 3rd ANS Topical Meeting on the Technology of Controlled Nuclear Fusion, Santa Fe, NM (May 9 - 11, 1978).

TABLE I SUMMARY OF PHYSICAL PROPERTIES

PROPERTY	H_2O COOLANT[a]	COPPER ALLOY (AMAX)	STAINLESS STEEL
Temperature T(O) (^oC)	250-300	250-350	400-500
Density, ρ (kg/m^3)	800	8800	8000
Viscosity, μ (Pa s)	$96(10)^{-6}$	-	-
Specific Heat Capacity, c_p (J/kg K)	5240	418	500
Thermal Conductivity, k (W/mK)	0.57	300	20
Prandtl Number, Pr ($\mu c_p/k$)	0.88	-	-
Melting Point, T_M (^oC)	-	1356	1703
Young's Modulus, E (GPa)	-	138	170
Coeff. Thermal Expansion, α ($10^6/K$)	-	16.5	18
Ultimate Tensile Strength, σ_U (MPa)	-	430	650
Yield Strength, σ_Y (MPa)	-	400	550
Thermal Stress Parameter, M (W/m)	-	70,000	5000

(a) Computer model actually uses temperature dependent properties from Reference 31.

TABLE II FUSION POWER-CORE PERFORMANCE COMPARISON

PARAMETER	STARFIRE[a]	MkIIB[a]	CRFPR	MARS
First wall radius, r_w(m)	2.83	2.71	0.75	0.60
Major radius, R_T(m)	7.0	6.7	3.8	131/214[c]
Nominal B/S thickness, Δb(m)	2.5	[3.2	0.60	0.84
Nominal coil thickness, Δc(m)	1.6		0.45	1.62
FPC volume, $V_{FPC}(m^3)$	8110 (6630)	8000 (4401)	242	11645
First-wall area, $A_{Fw}(m^2)$	780	716	112	494
FPC volume/surface, V_{FPC}/A_w(m)	10.4 (8.50)	11.2 (6.15)	2.16	23.6
System radius, $r_s(m) = (V_{FPC}/2\pi^2 R_T)^{\frac{1}{2}}$	7.66 (6.70)	7.78 (5.77)	1.60	4.2
Plasma chamber volume, $V_p(m^3)$	1106 (994)	970 (836)	42	148
Thermal power, P_{TH}(MWt)	4033	3260	3383	3400
Blanket energy multiplication, M_N	1.14	1.14	1.1	1.36
Recirculating power fraction, ε	0.167	0.08	0.16	0.22
Thermal conversion efficiency, η_{TH}	0.36	0.40	0.35	0.42
Neutron first-wall loading, I_w (MW/m^2)	3.6	3.2	19.5	4.3
System power density, P_{TH}/V_{FPC} (MWt/m^3)	0.50 (0.66)	0.41 (0.74)	14	0.29
Maximum system power density, $(M_N + 1/4)I_w/2r_w$(MWt/m^3)	0.88	0.82	17.55	5.77
FPC Mass, M_{FPC} (Tonne)	23174/16496	17330	1160	23308
. FW/B	1574	4700	223	31851
. S	13360/6682	3650	-	2980 (724)
. C	8240	8980[b]	937	8509 (3496)
FPC specific mass, M_{FPC}/A_{FW} (tonne/m^2)	29.7/21.2	24.2	10.4	47.2
FPC Cost (M$)	440.1/363.3	719.1 [473.9]	43.6	481
. FW/B	82.4	204.5 [135.0]	14.8	54
. S	186.1/109.3	137.2 [90.3]	-	56
. C	171.6	377.4 [248.6]	30.8	371
FPC mass utilisation, M_{FPC}/P_{TH} (tonne/MWt)	5.7/4.1	5.3	0.37	6.8
FPC density, M_{FPC}/V_{FPC} (tonne/m^3)	2.86/2.66	2.17 (3.94)	5.6	2.0
FPC unit cost, c_{FPC} ($/kg)	19.0/22.0	41.5 [27.3]	37.0	20.6
FPC volumetric cost, c_{FPC} (M$/m^3)	0.053/0.059	0.16 [0.11]	0.204	0.041
FPC area costs, $C_{FW} = (FPC\ cost)/A_w$ (M$/m^2)	0.66/0.51	1.00 [0.66]	0.36	0.97
Unit direct cost, UDC ($kWe)	1438	2556 [1685]	863	1480
Cost of electricity, COE (mills/kWeh)	67.0	-	40.7	TBD
Cost figures-of-merit				
. RPE/TDC	0.56	0.72	0.36	0.60
. FPC/TDC	0.26/0.21	0.23	0.06	0.20
. (FW/B)/TDC	0.05	0.067	0.017	0.30

(a) Values in parentheses based on elliptical volume, whereas otherwise volumes include central column. Values to right of slash do not include pumping ducts and ports. Values in brackets [ ] based on $ inflation whereas other corresponds to £ inflation from 1977 → 1980.

(b) does not include mass of 35,000 tonne iron core.

(c) central-cell length/total length (includes end cells and direct collectors).

TABLE III SUMMARY OF BASE CASE CONDITIONS

First wall material	Copper	Steel
Peak Temperature, T(O) (^{o}C)	350	450
Coolant outlet temperature, T_c (^{o}C)	282[a]	
Sub-cooling, ΔT_{SAT} (K)	30[a]	
Tube inside diameter, d (mm)	20	
Volumetric nuclear heating, q/I_w [(MW/m^3)/(MW/m^2)]	10	
Blanket energy multiplication, M_N	1.17[b]	

(a) corresponds to a coolant pressure of 10 MPa
(b) corresponds to 20 MeV per fusion event

TABLE IV SUMMARY OF COSTING PARAMETERS ADOPTED FOR BASE CASE

Net electrical power output, P_E (MWe)	1000
Radiation damage lifetime, $I_w\tau$ (MWyr/m^2)	15
FPC area cost, c_{FW} (M$/m^2)	0.5
Fraction of direct costs attributed to first wall, blanket and shield, $f_{FW/B/S}$	0.015
Baseline recirculating power fraction, ε_o	0.10
Temperature of Intermediate Heat Exchanger, T_{IHX} (^{o}C)	470
Pumping efficiency, η_{pump}	75%

List of Notation

Δb	Blanket/shield thickness
c_{FPC}	Cost per unit volume of FPC
c_{FW}	Cost per unit area of FPC
c_p	Coolant specific heat capacity
Δc	Coil thickness
d	First wall coolant tube inside diameter
E	Young's modulus
f_{CHF}	Geometrical enhancement factor for CHF
f_F	Fanning friction factor
f_{FW}	Fraction of total fusion energy deposited in first wall tube array
$f_{FW/B/S}$	Fraction of direct costs attributable to first wall, limiter
f_{RAD}	Fraction of alpha power radiated
h	Heat transfer coefficient
I_{QW}	Heat flux incident on first wall
I_W	Fusion neutron first wall loading
$I_W\tau$	First wall radiation damage lifetime
I_α	Total power flux at plasma edge
k_c	Coolant thermal conductivity
k_w	Tube-wall thermal conductivity
L	Heated length of coolant tube
M	Thermal stress parameter
M_N	Blanket energy multiplication factor
N	Number of first wall coolant tubes
N_c	Design number of cycles
P_f	Plant factor
P_c	Coolant pressure
P_E	Net electrical power output
P_{ET}	Gross electrical power output
P_{TH}	Total thermal power output
Pr	Prandtl number
q	Volumetric power density in tube-wall
r_s	System minor radius
r_w	First wall minor radius
R_T	Major radius

Re	Reynolds number
S_m	Maximum allowable time-independent primary stress
T_{BLK}	Blanket coolant temperature
T_c	Coolant outlet temperature
T_{IHX}	Intermediate Heat Exchanger fluid temperature
T_{SAT}	Coolant saturation temperature
$T(O)$	Peak tube-wall temperature
$T(\delta)$	Inner tube-wall temperature
ΔT_f	Film temperature drop
ΔT_{IHX}	Temperature differences across Intermediate Heat Exchanger
ΔT_{SAT}	Coolant sub-cooling
ΔT_W	Temperature drop through tube-wall
u	Coolant velocity
V_{FPC}	Fusion Power Core volume
X	Normalised primary stress
Y	Normalised secondary stress
α	Coefficient of thermal expansion
δ	Coolant tube wall thickness
ε	Recirculating power fraction
ε_o	Minimum recirculating power fraction
ε_p	Ratio of first wall coolant pumping power to total thermal power
ε_{TH}	Cyclic thermal strain
η_p	Overall plant efficiency
η_{PUMP}	Pump efficiency
η_{TH}	Overall thermal efficiency
κ_c	Coolant thermal diffusivity
μ_c	Coolant viscosity
ν	Poisson's ratio
ξ	Factor in thick-walled-tube model
ρ_c	Coolant density
σ_c	Effective creep stress
σ_p	Primary (pressure) stress
σ_{TH}	Secondary (thermal) stress
σ_u	Ultimate tensile strength
σ_Y	Yield stress

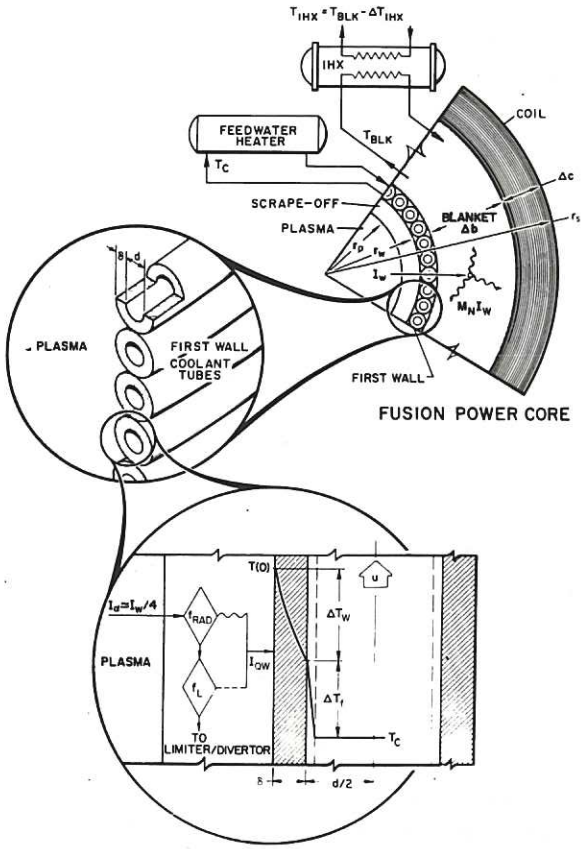

Fig. 1 First wall thermal-mechanical model and identification of key notation.

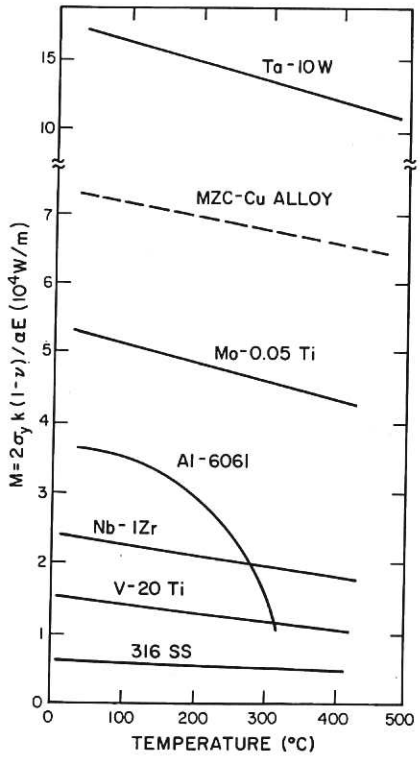

Fig. 2 Temperature dependence of stress parameter, M, for a range of engineering alloys.

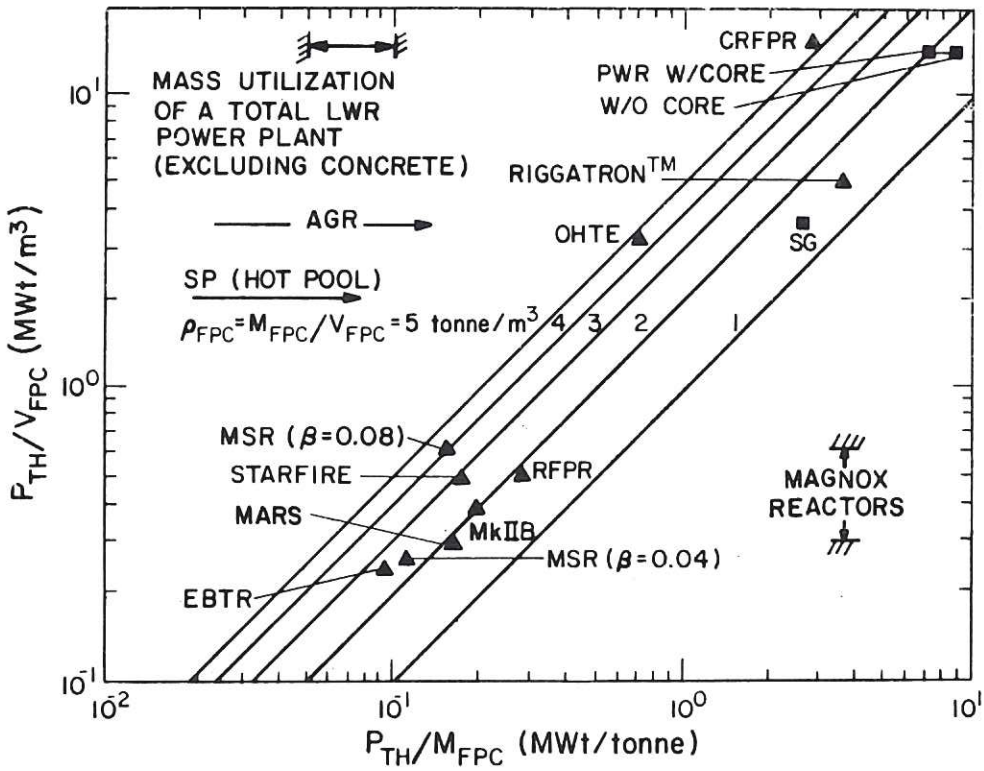

Fig.3 Summary of system power densities being projected by a number of recent fusion reactor designs, indicating the range of average or "smear" density for the FPC: STARFIRE [24]; ELMO Bumpy Torus, EBTR [36]; Modular Stellarator Reactor, MSR [37]; Pressurised Water Reactor, PWR, and Steam Generator, SG [38]; Ohmically Heated Torus Experiment, OHTE [39]; Reversed Field Pinch Reactor, RFPR [40]; Compact RFP Reactor, CRFPR [26]; Riggatron Tokamak [41, 42]; Culham MkIIB Tokamak, MkIIB [27, 43].

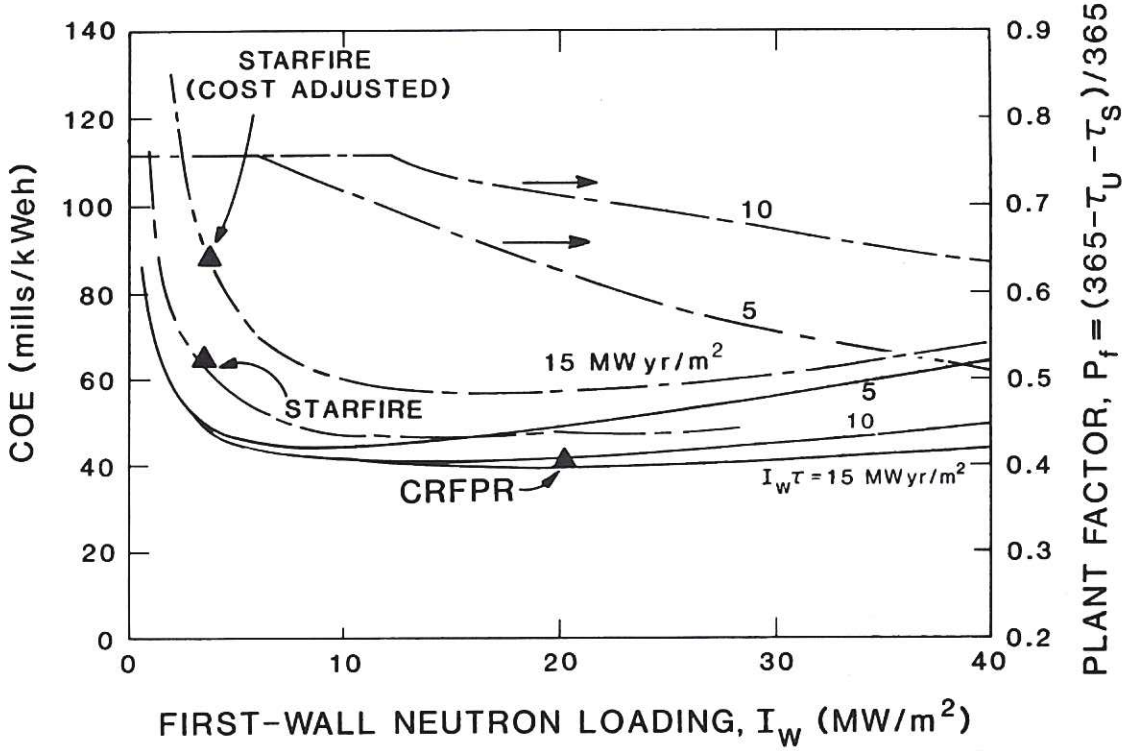

Fig.4 Dependence of COE (mills/kWeh) on fusion neutron wall loading, I_w (MW/m^2) for a compact and a superconducting coil fusion reactor using equations 20 and 22 and the composite data given in Table II.

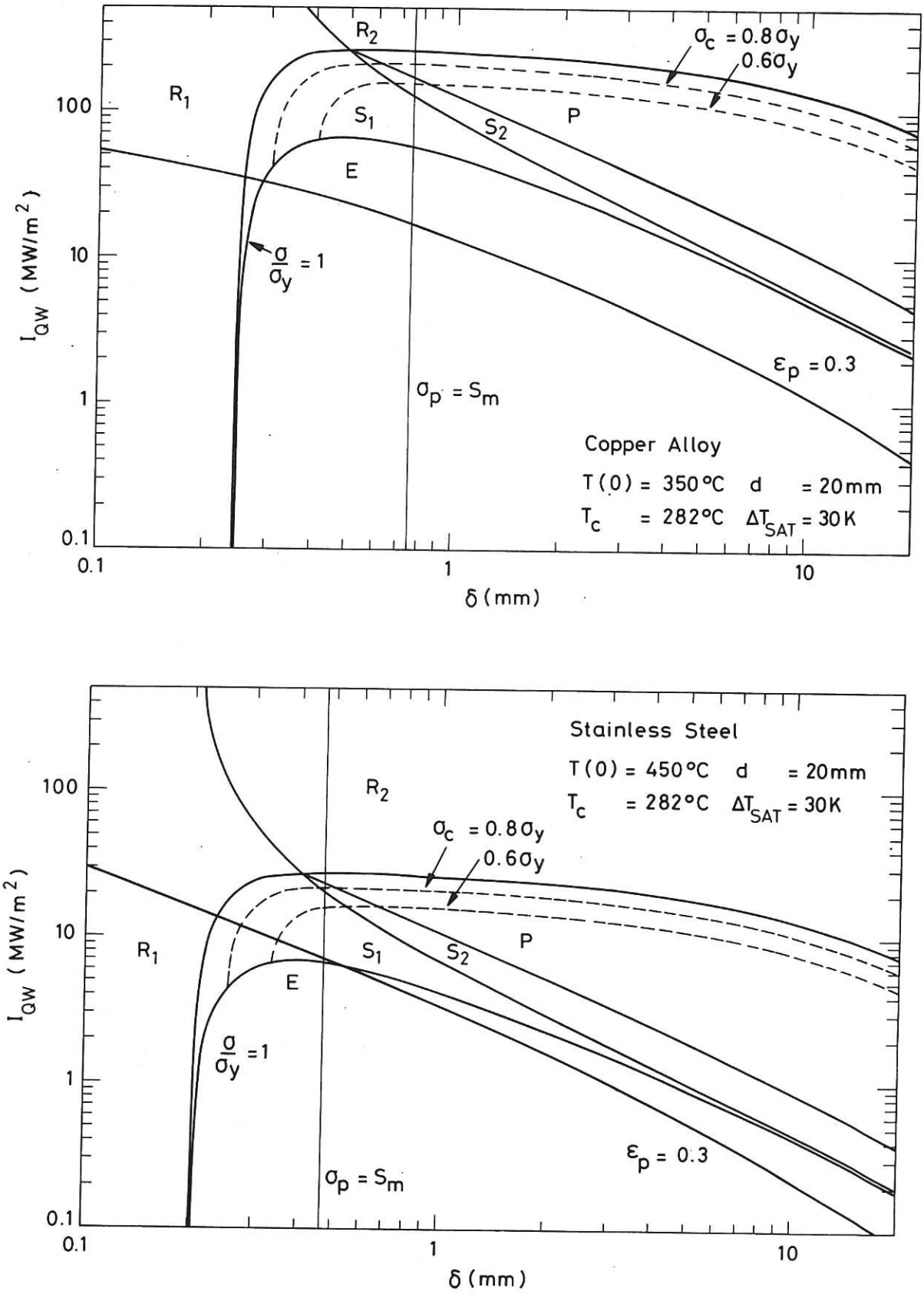

Fig.5 Modified Bree diagram plot of surface heat flux versus wall thickness for copper alloy and stainless steel showing effective creep stress contours and constraints on pumping power and primary stress.

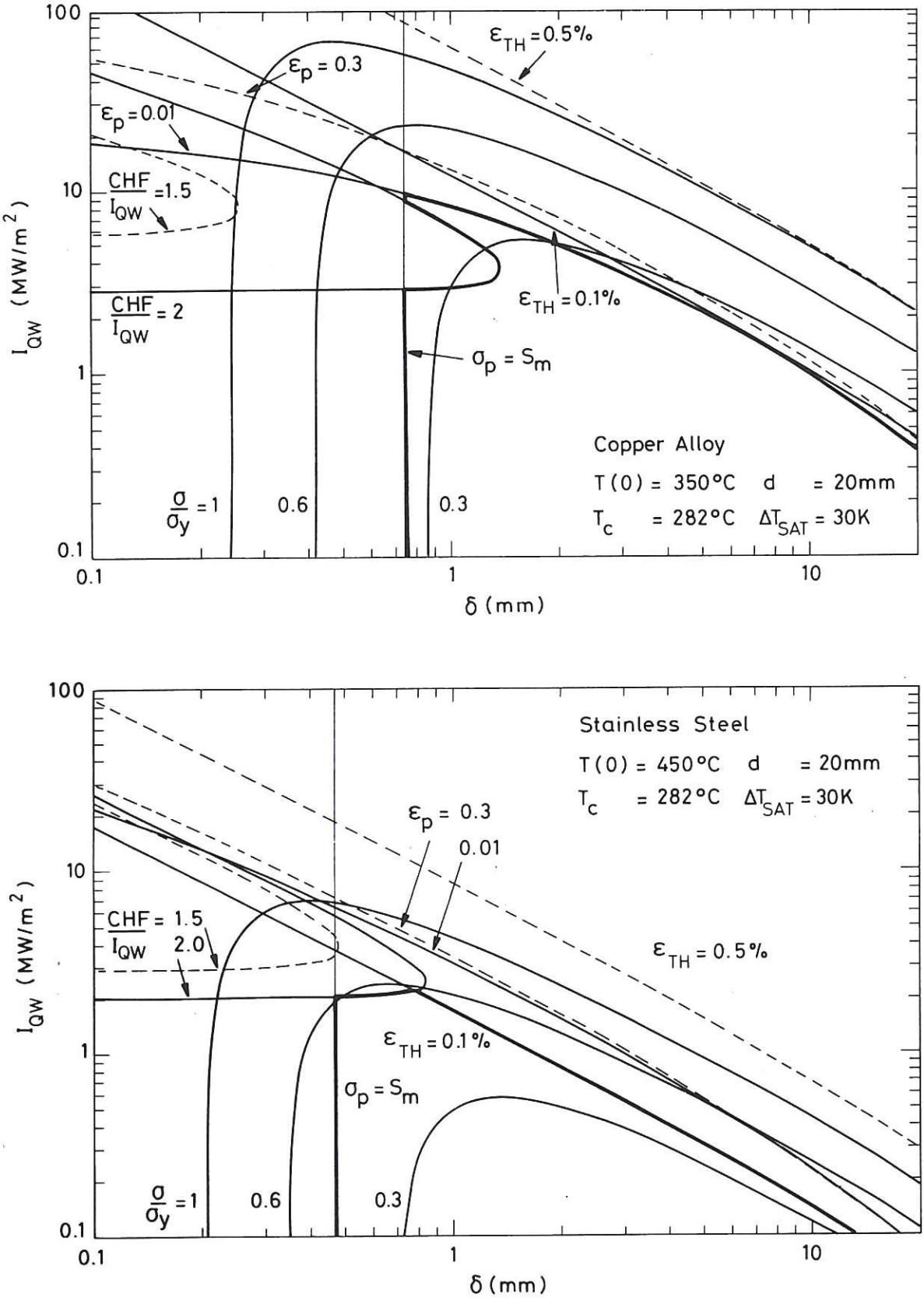

Fig.6 Surface heat flux versus wall thickness plot for copper alloy and stainless steel showing contours of constant σ/σ_Y, ϵ_p, ϵ_{TH}, CHF/I_{QW} and constraint on primary stress.

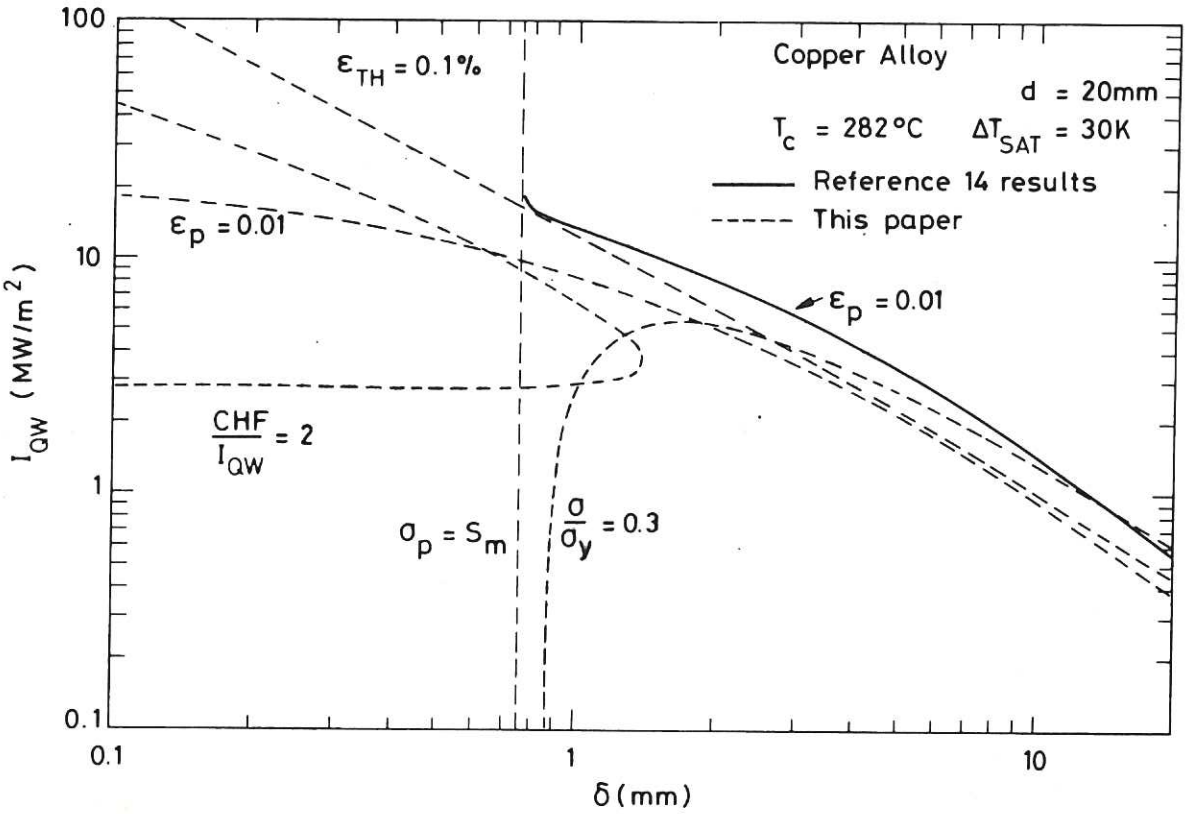

Fig.7 Surface heat flux versus wall thickness for copper alloy comparing results of Reference 14 with this paper for the base case operating conditions.

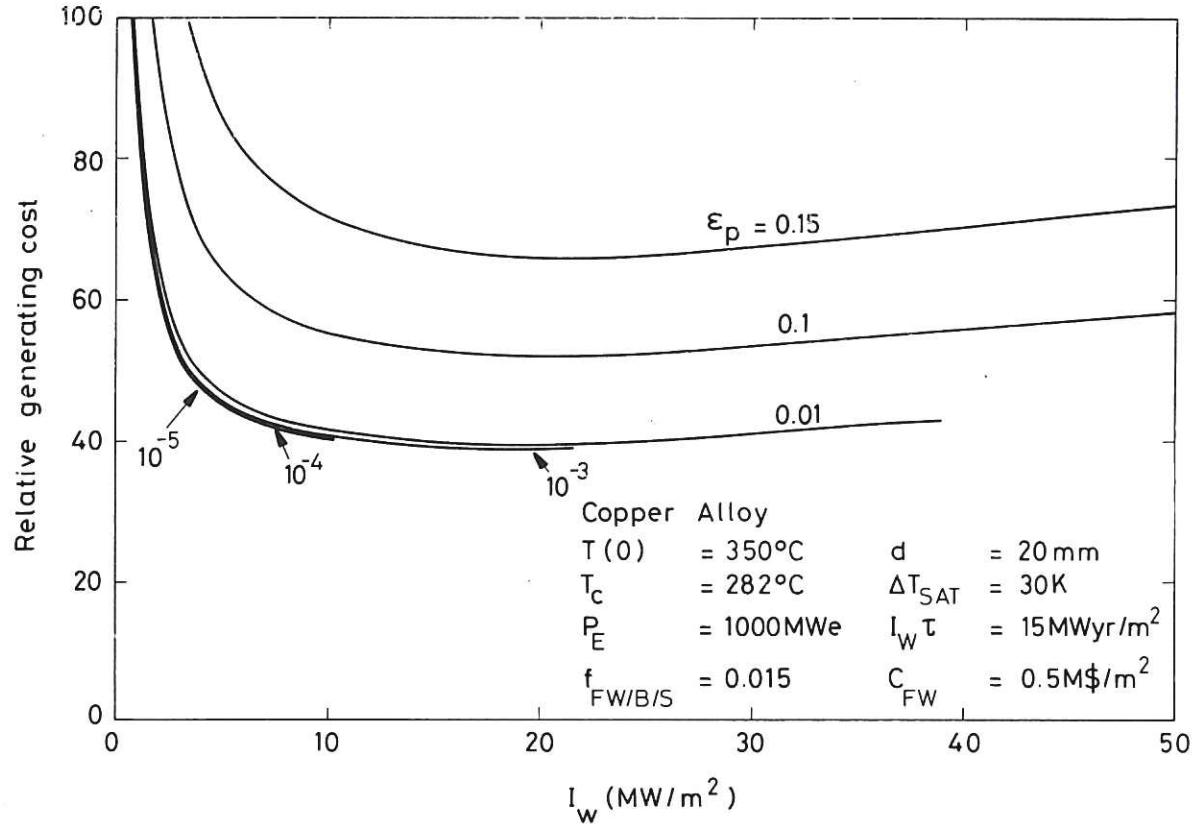

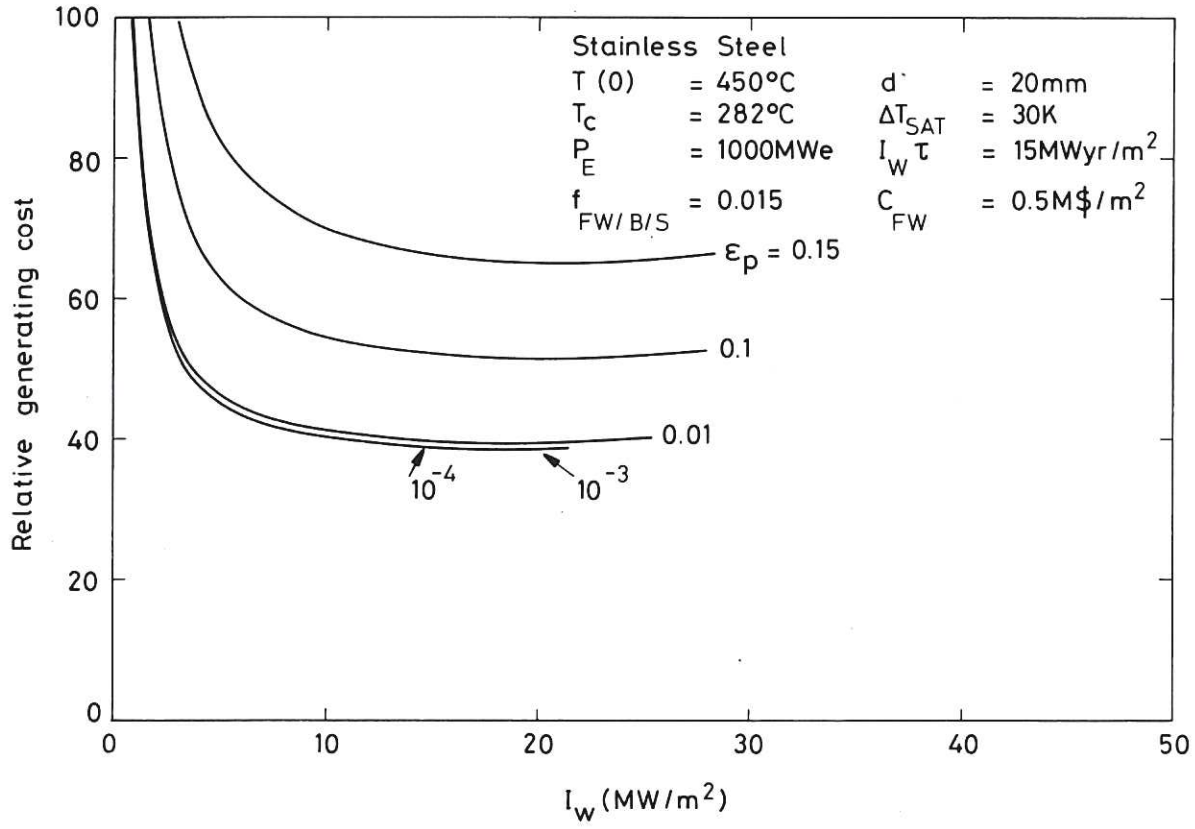

Fig.8 Relative generating cost as a function of neutron wall loading for copper alloy and stainless steel for various values of ϵ_p.

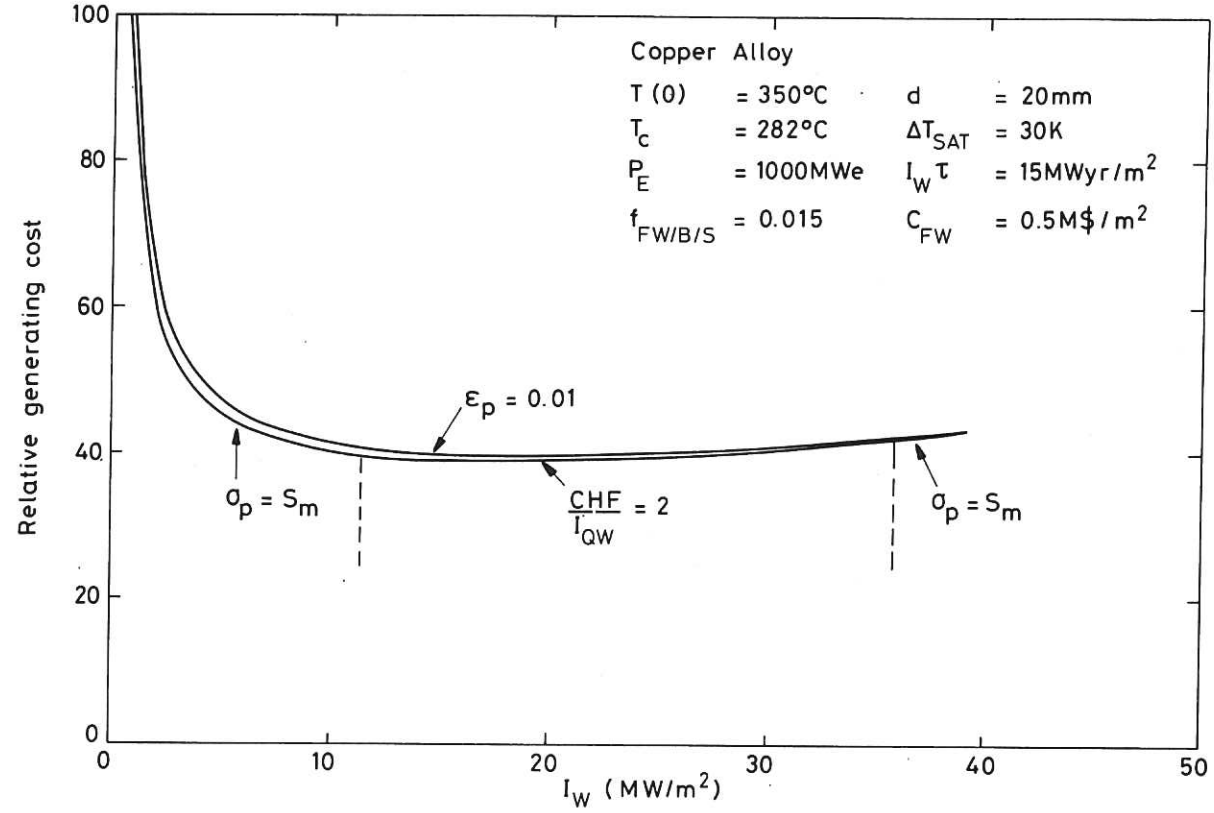

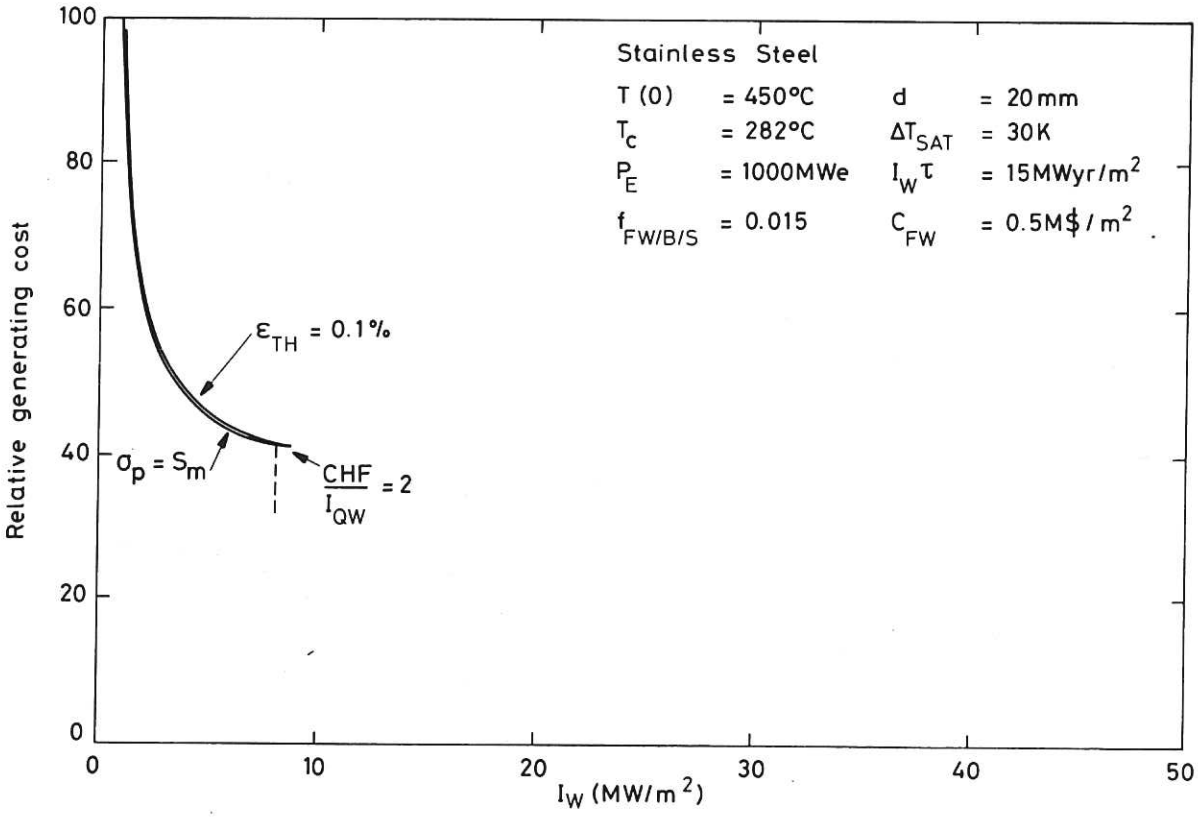

Fig.9 Relative generating cost as a function of neutron wall loading for copper alloy and stainless steel at all points of the boundary of the design window shown in Fig.6.

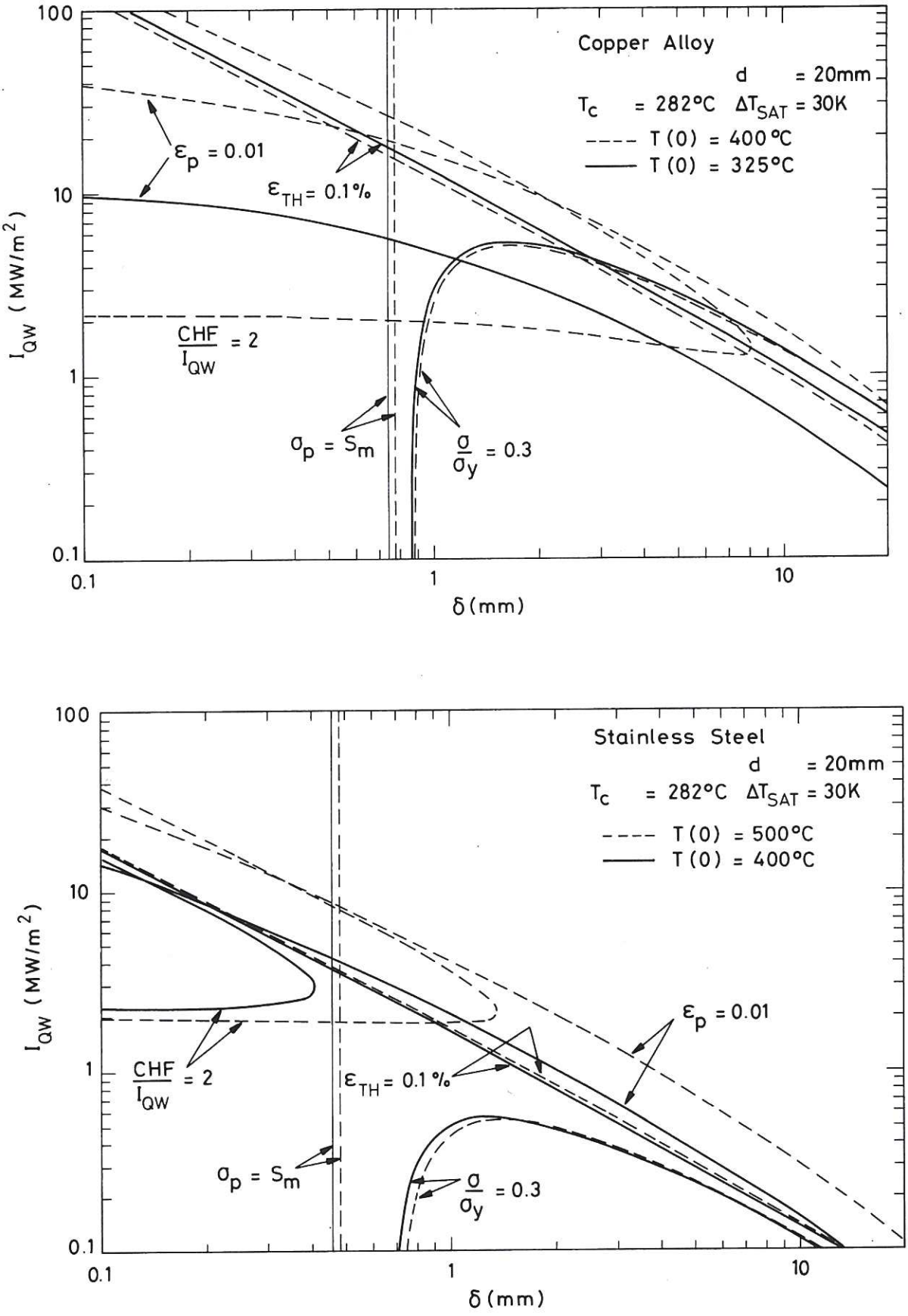

Fig. 10 Surface heat flux versus wall thickness for copper alloy and stainless steel showing effect of varying material temperature on ϵ_p, ϵ_{TH}, CHF, σ/σ_Y and primary stress constraints.

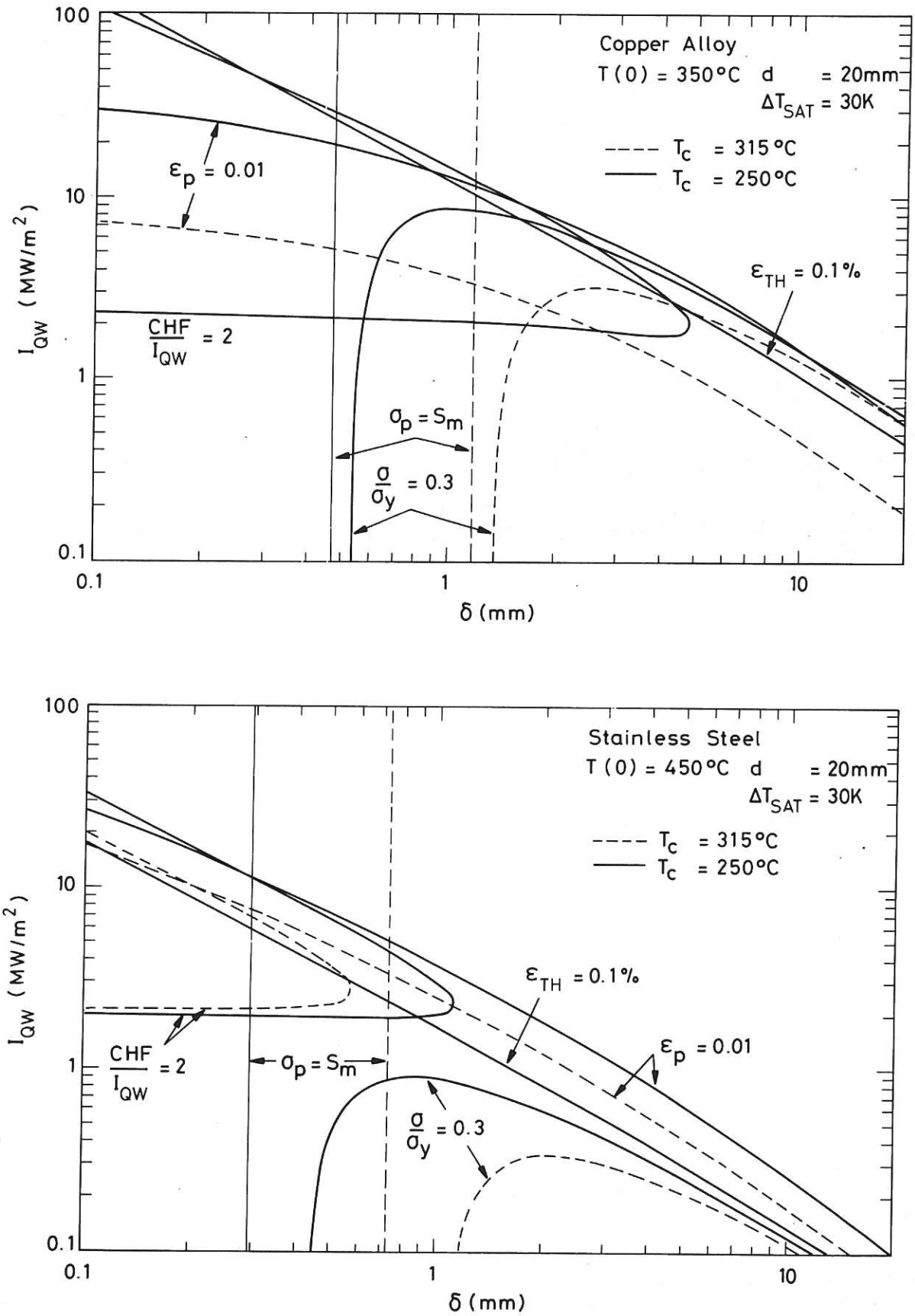

Fig. 11 Surface heat flux versus wall thickness for copper alloy and stainless steel showing effect of varying coolant temperature on ϵ_p, ϵ_{TH}, CHF, σ/σ_Y and primary stress constraints.

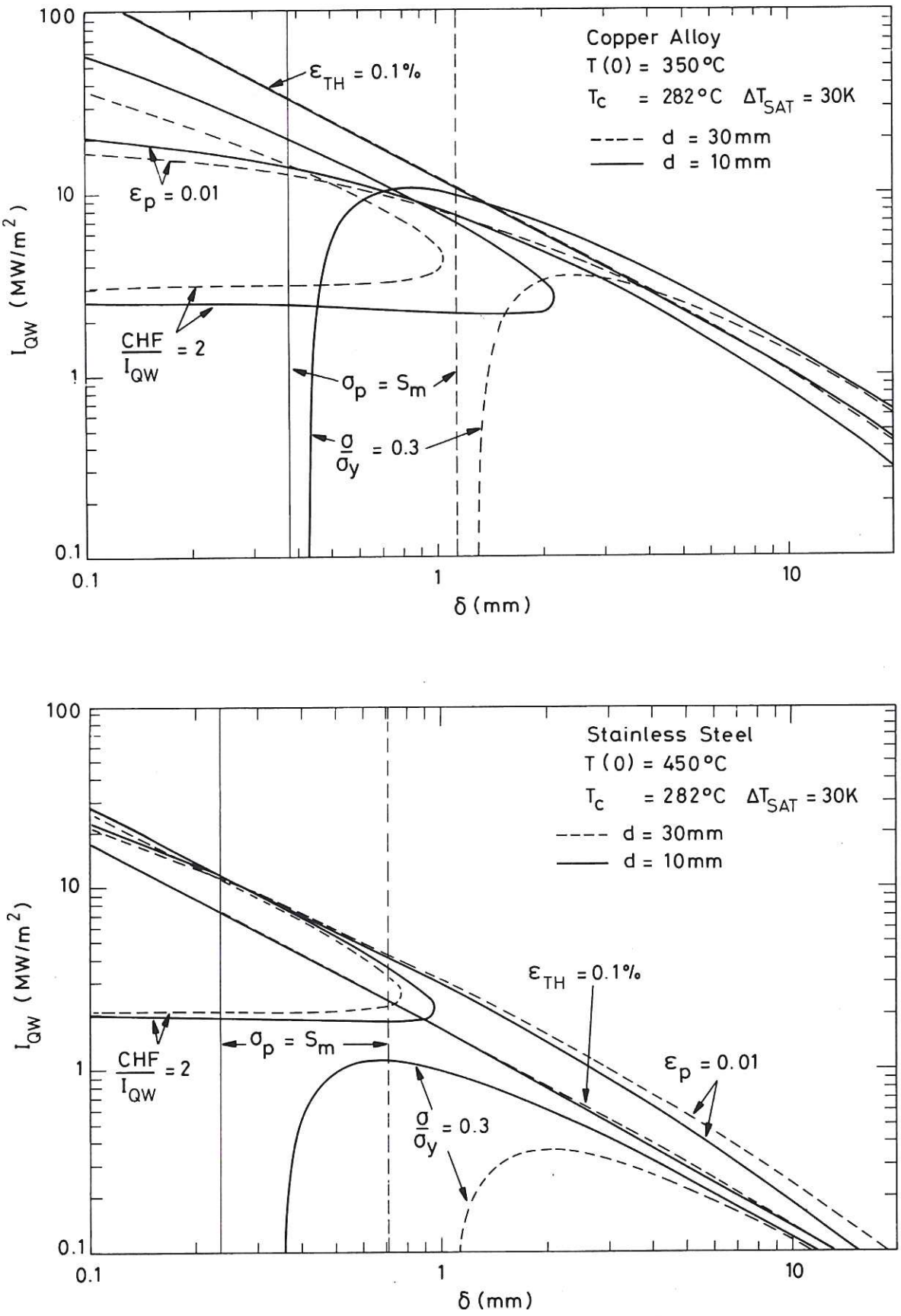

Fig. 12 Surface heat flux versus wall thickness for copper alloy and stainless steel showing effect of varying tube diameter on ϵ_p, ϵ_{TH}, CHF, σ/σ_Y and primary stress constraints.

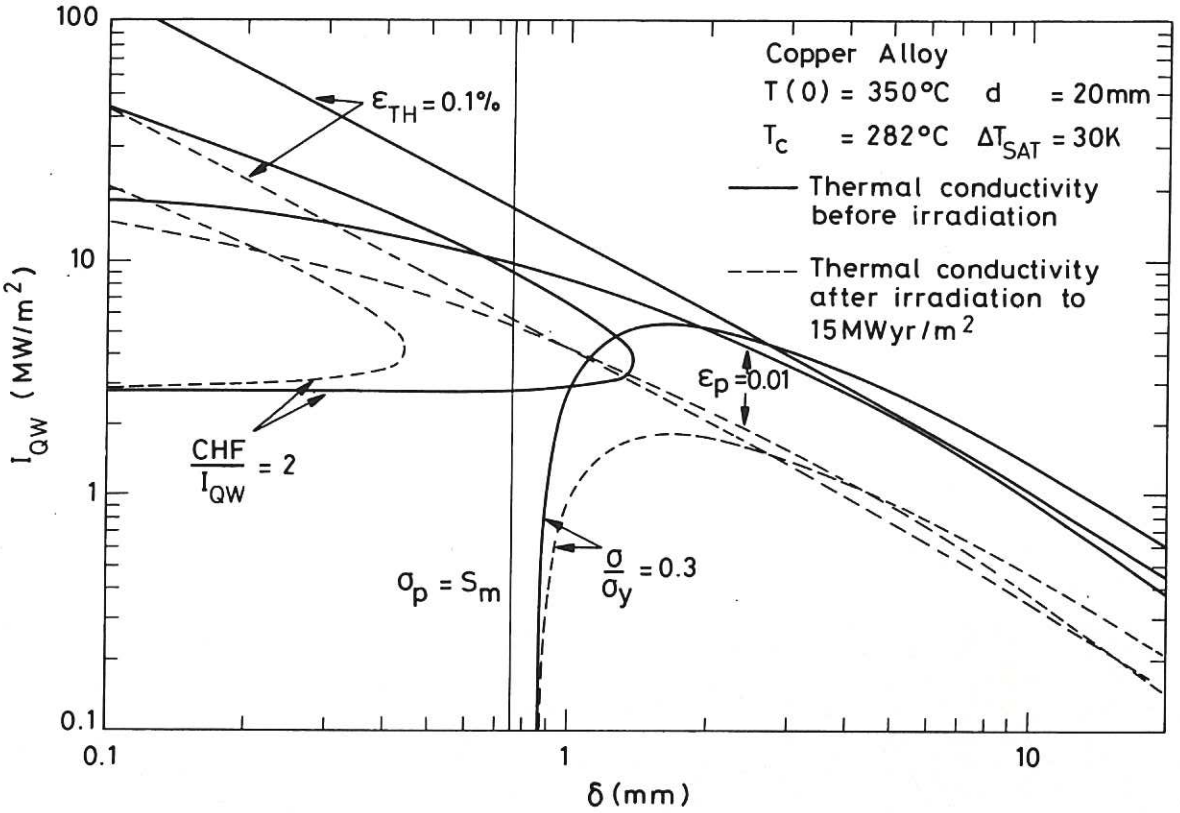

Fig. 13 Surface heat flux versus wall thickness for copper alloy first wall showing the effect on the base-case response (Fig. 6) for end of life transmutation product build-up.

HER MAJESTY'S STATIONERY OFFICE

Government Bookshops

49 High Holborn, London WC1V 6HB
(London post orders: PO Box 276, London SW8 5DT)
13a Castle Street, Edinburgh EH2 3AR
Brazennose Street, Manchester M60 8AS
Southey House, Wine Street, Bristol BS1 2BQ
258 Broad Street, Birmingham B1 2HE
80 Chichester Street, Belfast BT1 4JY

Publications may also be ordered through any bookseller